POLITECNICO DI TORINO

Master's Degree in Energy and Nuclear Engineering

Master's Degree Thesis

Optimal exploration of renewable resources for supporting energy transition

Supervisors

Prof. Tao HUANG

Prof. Alessandro CIOCIA

Candidate

Juan Manuel BASTO LÓPEZ

Academic Year 2022/2023

Summary

The depletion of fossil fuel resources and the environmental damage associated with their use have prompted the development and emergence of new energy systems based on renewable energy sources (RES) in the 21st century. In this thesis, an optimal planning approach for renewable energy systems is proposed based on the maximization of self-sufficiency. The planning strategy aims to ensure that a single region or multiple adjacent regions can meet their energy needs primarily through RES while utilizing the electricity grid for power exchange among them. The objective is to develop a Python-based tool to estimate the potential of RES and find the optimal wind and photovoltaic generation and storage capacities that satisfy power and energy balance and grid constraints at the hourly level while maintaining a certain level of economic benefits. In order to achieve it, two optimization models are formulated according to whether the analysis concerns a single-site or multiple-sites. In the former case, the objective function is converted to the minimization of power absorption from the grid. For the latter one, electrical grid constraints are added to model power flow and relevant grid constraints. The tool intention is to support decision and policy makers to easily create and analyse different energy scenarios with an hourly resolution, for a time frame no longer than 25 years.

As a case study, Sardinia Island is selected for the years 2030 and 2050. The final simulation results highlight the level of self-sufficiency from provincial to island level for a 21-year period, ensuring an internal rate of return (IRR) greater or equal to 8%, having a positive return of the initial investment at the end of the useful lifetime of installed renewable energy systems.

Acknowledgements

At the end of this Master Thesis and my Double Degree program I would like to thank all the people who has supported me throughout this learning journey.

I am really thankful for the valuable time and knowledge my supervisors *Prof. Tao Huang* and *Prof. Alessandro Ciocia* shared with me during this period.

I am grateful to my friends in Turin, who made me feel like home since then.

Thanks to my brother, friend and master's colleague Joseph, the one who always reminded me this was more than possible.

Finally, I would like to thank my family for their endless love since the very beginning. Particularly to the ones who inspire me everyday: my sister and dad.

And obviously mom, this is especially dedicated to you and your legacy.

Contents

List of Tables

List of Figures

Acronyms

RES
Renewable energy sources

IEA
International Energy Agency

SS
Self-sufficiency

SC
Self-consumption

PV
Photovoltaic

WT
Wind Turbine

BESS
Battery Energy Storage System

PSH
Pumped Storage Hydropowe

CAES
Compressed Air Energy Storage

UPS

Unstoppable power supply

PPS

Production Peak shaving

SOC

State of Charge

NPV

Net present value

DERs

Distributed energy resources

STC

Standard test conditions

AM

Air mass

NOCT

Normal Operating Cell Temperature

V2G

vehicle-to-grid

EES

Electrical Energy Storage

LIB

Lithium ion batteries

DC

Direct Current

AC

Alternate Current

TRL

Technology Readiness Level

SOH

State of health

OM

Operation and maintenance

MIQP

Mix-integer Quadratic Programming

MILP

Mix-integer Linear Programming

HVDC

High-voltage direc current

PTDF

Power Transfer Distribution Factors

DAO

Data access object

CA

Cagliari

CI

Carbonia Iglesias

SSS

Sassari

OG

Ogliastra

OT

Olbia Tempio

OR

Oristano

VS

Medio Campidano

NU

Nuoro

nPV

Number of PV panels

nWT

Number of wind turbines

List of Symbols

α	Angle of attack (°)
η	Efficiency
γ	Power reduction coefficient ($\%/°C$)
λ	Tip speed ratio (m/s)
ρ	Reflection coefficient
A	Area (m^2)
B	Susceptance (S)
Cs	Storage capacity (kWh)
E	Energy (kWh)
f	Frequency (Hz)
G	Solar irradiance (W/m^2)
I	Electric current (A)
M	Big M variable
P	Power (W)
R	Electric Resistance (Ω)
S	Binary decision variable
T	Temperature ($°C$)
U	Electric Voltage (V)
u	Wind speed (m/s)

X Reactance (Ω)

Z_0 Terrain roughness (m)

Introduction

Energy is often referred to as the "universal currency" because it can be transformed and exchanged between different forms to get anything done. It is a crucial aspect of many natural and technological systems and plays a central role in modern society [1]. However, the major source of energy supply still relies on fossil fuels, which have several negative environmental consequences. These impacts have pushed for the increased use of renewable energy sources (RES) to transition to a more sustainable energy system. Unlike fossil fuels, these sources are inherently sustainable, with significantly lower or zero greenhouse gas emissions and reduced environmental impact.

Promoting the rapid growth of an emerging energy system that is based on RES and proposes a paradigm shift on how consumers and enterprises interact can be challenging. In order to achieve a well-driven energy transition, both decision and policy makers, should take into account different variables to accurately tackle the climate and energy crisis within the development of energy policies [2]. These variables should not only benefit the reliability of the energy system by increasing its efficiency or upgrading technologies but, supporting the perfect competition inside the energy market for all players, including prosumers. This concept is a game-changer inside the energy industry, it proposes to move from an historically centralized approach of energy supply to a decentralized one, giving the possibility to consumers to produce energy and trade it inside the energy market.

Due to the fact, Distributed Energy Resources (DER) are being promoted inside the emerging energy systems to support local generation and consumption, and incentives players to actively engage energy transition. Two well-defined energy indicators that are characteristic from DER systems are Self-sufficiency (SS) and Self-consumption (SC), which quantify the exploitation of energy generation at local level. Certainly, by enhancing both indicators the energy scenarios can be positive affected and triggered towards a reliable energy landscape.

Indeed, this is the motivation for this thesis; select an energy indicator that encompasses different variables inside the energy system by its own, ensuring that captures multiple aspects that are favorable to the energy transition, thus, in alliance with decision and policy makers prospective. In this work, SS is chosen as such indicator by maximizing it, it is possible to plan and model energy scenarios that are in accordance with the energy transition goals and can support founded decision-making.

This thesis proposes a single-objective optimization model which maximizes SS in order to obtain the optimal energy generation from RES and energy storage capacities that satisfy power balance, electrical network and economic constraints. The model encompasses energy scenarios within a single-site or multiple-site approach. Having electricity as its only energy carrier, the model allows the power sharing between RES generation, electrochemical storage and the power grid. The multiple-site is modelled considering the electrical grid as the interconnected paths between individual sites.

The work done in [3] has been employed as a framework for this thesis. The purpose is to develop an open-source tool that supports decision-making by easily creating energy scenarios, built from a linearized optimization model that enables the straightforward implementation of Linear Programming (LP). In this sense, computational cost is decreased and large dataset handling is achieved.

The program has been built within the Python environment and the integration of the powerful mathematical programming solver Gurobi, alongside a graphic unit interface (GUI) the tool enables users to easily create energy scenarios and then, interactively visualize and analyze results. Optimal planning of renewable energy systems and the design of energy scenarios is hence a significant topic for energy planners and decision-makers. The tool aims to support decision and policy makers to take founded decisions from regional to country level approaches.

In addition, the tool is tested in a case study: The green electrification of Sardinia. The Italian Island is nowadays gathering big attention from global entities, regarding the worldwide target of decarbonization. They are aiming to effect a drastic change in Sardinia's energy model by 2030, gradually eliminating production from fossil fuels and increasing the proportion of energy produced from photovoltaic and wind power [4]. Therefore, the energy landscape in Sardinia is emerging from conventional fossil fuel generation to renewable energy systems, which makes it ideal to test the tool.

Chapter 1

Renewable generation for energy transition

Over the past decade, an issue of strong international interest both inside and outside the energy sector is undoubtedly climate change. The European Commission has embarked on a long-term strategy confirming its intention to implement global action to counter the effects of climate change. The goal is to achieve net zero[1] by 2050 through a socially equitable and economically efficient energy transition, developing a sustainable energy with the implementation of renewable energy sources (RES) [5].

It is strongly advised that countries change their energy consumption policies toward RES by investing in renewable energy technologies and research for more sustainable growth [7]. As a matter of fact, The period from 2020 to 2030 holds significant importance in pursuing the net zero target. It is imperative to utilize this decade for thorough preparation and strategic planning, aiming to accomplish complete reliance on RES across all sectors.[8]. In figure 1.2 is illustrated the increasing energy generation from renewable and the unstoppable decay of traditional generation with projected data by the International Energy Agency (IEA) up to year 2027.

This mitigation should be addressed by implementing current developed technology and high level optimization techniques and optimal planning analysis. "By the hand of digitalization, energy systems should be positive stimulated to increase

[1] zero greenhouse gas emissions

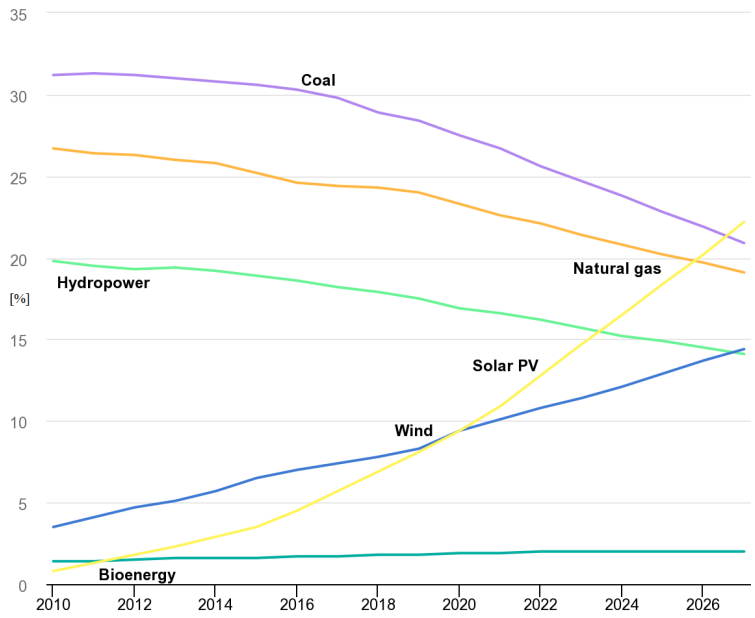

Figure 1.1: Share of cumulative power capacity by technology from 2010 to 2027 [6]

their efficiencies by optimizing consumption and metering, reducing losses, generate energy with the lowest costs and emissions" [9]. Furthermore, leveraging the historical momentum of renewable energy capacity growth, primarily driven by photovoltaic and wind technologies, IEA projects a significant milestone in Figure 1.1. According to the data, by 2027, RES will surpass all other forms of power generation in terms of global cumulative capacity. This achievement would mark the first time in history that renewables will take the lead in meeting the world's energy needs, heading to meet a reliable energy transition [6].

Nevertheless, RES is affected by the intermittency issues related to their fluctuating behavior, also by their bounded availability, and economic obstacles. This means the increase on energy system's complexity, which requires the proper examination of different variables in order to identify viable configurations. It is well known that the day-to-day observation and optimization of the existing energy systems is crucial to get their desired well-functioning. However, planning and optimal sizing the capacities from generation and storage sides are crucial for the implementation of RES technologies in the current energy scenarios. Furthermore, optimizing an energy system can be expressed as a single-objective or multi-objective optimization problem. However, it is more practical to frame the problem as multi-dimensional [10].

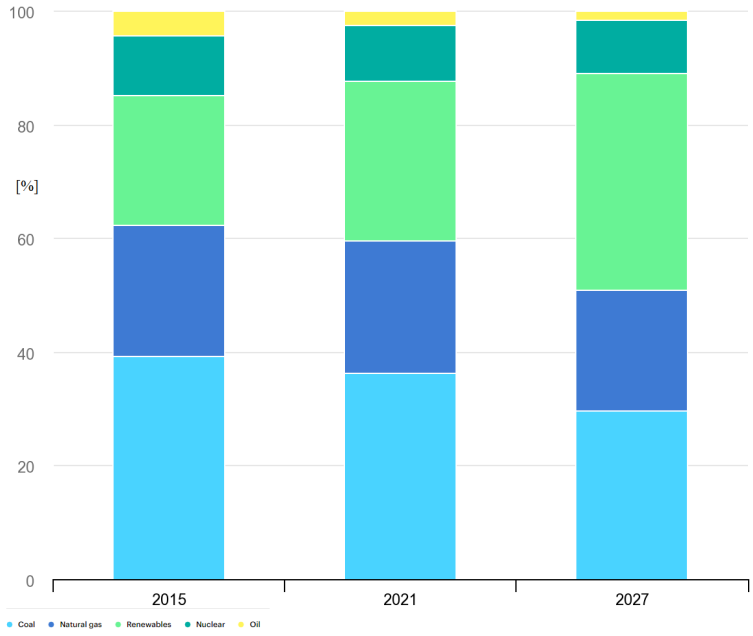

Figure 1.2: Global electricity generation by technology, 2015, 2021, and 2027. [6]

The scope of this research is limited to the analysis of a single energy carrier, specifically electricity, with a focus on single-objective optimization. The objective is to maximize self-sufficiency by optimal sizing generation and storage capacity while meeting economic and power balance constraints. Moreover, linearizing the optimization problem using advanced techniques and solvers. One of the goals is to achieve convergence with minimal computational and timing costs, even when working with large datasets. Section 3 provides a more detailed explanation of the energy models and optimization procedures used in this research. The following subsection highlights the significance of self-sufficiency in renewable energy systems and outlines how this research aims to maximize it.

1.1 Significance of Self-sufficiency and strategies to its maximization

In recent years, the concept of self-sufficiency has garnered a lot of attention, particularly in the area of energy systems. Individuals, communities, and even entire nations may generate, manage, and use their own energy resources without relying heavily on external sources. It is a paradigm shift away from the old

centralized energy approaches and towards more decentralized and sustainable alternatives. The success of the self-sufficiency model is justified by the fact that in an increasing number of countries, renewable energy, and in particular photovoltaics, has achieved a unit cost of electricity generated that is equal to or less than the unit cost of electricity consumed from the grid. Grid parity allows users to save money by generating their own power rather than purchasing it from the grid [11].

Self-sufficiency (SS) is an energy indicator to quantify the exploitation of energy generation at local level, is defined as the amount of electricity locally generated and consumed (E_{lgc}) with respect to the the total demand (E_{load}). It measures user independence from the grid [12]. Another important indicatator that comes along is Self-consumption (SC) which refers to the proportion of E_{lgc} to total local generation (E_{gen}) [13] and both are determined by:

$$SS(t) = \frac{E_{lgc}(t)}{E_{load}(t)} \tag{1.1}$$

$$SC(t) = \frac{E_{lgc}(t)}{E_{gen}(t)} \tag{1.2}$$

where t is the time interval over which the ratio is calculated hourly, daily, monthly, or annually [14]. In Figure 1.3 are shown hourly general profiles of power generation, in this case only Photovoltaics (PV), and the power consumption of a domestic user. In the hours of maximum production when generation exceeds consumption and assuming there is no storage integration within the system, the surplus energy can either be wasted or injected to the grid. This interval case means to low levels of SC but achieving high levels of SS because the load has been satisfied by the local generation.

High levels of both energy indicators are crucial for emerging energy systems that delve the path for energy transition. Accordingly, descentralized energy generation approaches are being addressed to tackle climate change, as a consequence sustainable local energy markets and new players denominated prosumers[2] are being part of the emerging energy trading, where communities can balance generation and consumption locally [15]. Therefore, the strategies to maximize SS assist the energy scenarios that are triggering the energy transition and the emerging electricity market that comes along. The following arguments deep inside the main strategies that are being adopted to maximize SS and SC.

[2]Individuals or entities that actively participate in the energy market as both producers and consumers of energy

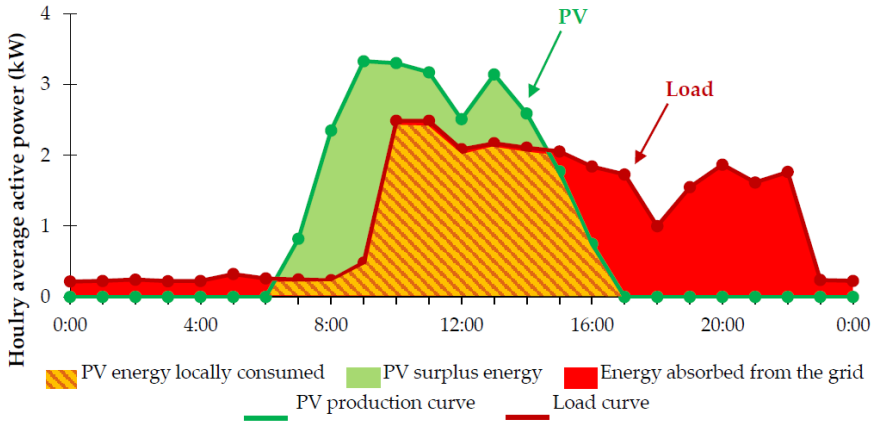

Figure 1.3: Generic example of PV generation and load profiles of a domestic user. [14]

1.1.1 Implement energy storage systems

Many methods for achieving high degrees of self-sufficiency and self-consumption are available, the integration of energy storage is the most popular approach for increasing their levels. Technologies such as Battery Energy Storage System (BESS), Pumped Storage Hydropower (PSH) or Compressed Air Energy Storage (CAES), are systems that store excess energy generated during periods of low demand or high generation and release it when needed, ensuring a reliable and unstoppable power supply (UPS). Energy storage addresses the intermittency issue that most renewable energy generation present, it is projected that the deployment of energy storage technology would boost supply while balancing demand for energy [16]. Nonetheless, the capital costs of energy storage systems is nowadays still high, generally represent a significant portion of the overall project cost due to their specialized components and infrastructure requirements.

In Figure 1.4 are illustrated the main energy storage technologies, with their main features of operation. Their implementation are based on the capacity they can manage, location of generation plant and time response. For example PHS and CAES technologies are large-scale intermittent balancing with high level of storage capacity but are not able to compete frequency response market due to their low discharge time. In contrast Hydrogen-based storage solutions are the only technology able to address the intermittency balancing at high penetration levels. Batteries instead, in chemical and flow composition are competing for broader power and energy ranges with different times of discharge and response that can provide flexibility to the dis-match of demand and supply [17].

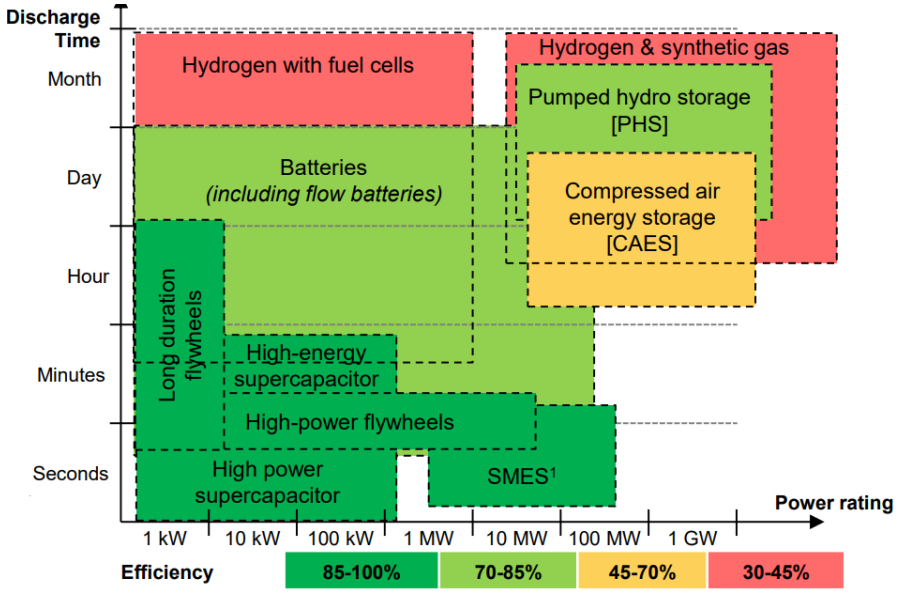

Figure 1.4: Electricity storage technologies' features [17]

Undoubtedly, energy storage is fundamental for the maximization of SS in the context renewables energy systems where production and consumption patterns often do not align. The mitigation of the intermittency balancing carried out by storage technologies gives flexibility to the emerging energy systems and expanding the possibilities of trade in new energy markets and giving productive final use of the surplus energy storing it or injecting it to the grid in order to reduce curtailment. Electrochemical storage systems, such as batteries, are highly implemented for Peak shaving strategies, which tackle the intermittency issue by adjusting either the production (production peak shaving) or the consumption profiles (demand peak shaving) to obtain better profiles matches, avoiding injecting to the grid. Thus, increasing SC. Nonetheless, it is also possible to achive the same effect without implementing storage systems [14].

1.1.2 Optimize generation and demand management

Promoting energy-efficient practices and implementing demand-side management strategies can help balance energy consumption and generation. By incentivizing energy conservation, shifting peak demand, and utilizing smart grid technologies. SS and SC can be improved by reducing the overall energy demand and avoiding the need for additional generation or storage capacity.

Two well-known of these strategies refer to Peak shaving; either on production (PPS) or demand (DPS). The first, involves intentionally reducing the energy generated by RES to prevent overload and overvoltage events while providing significant advantages to the electricity grid. By implementing PPS, the aim is to maintain grid stability and avoid potential issues caused by excessive energy production from RES. This approach ensures a valuable contribution to the overall performance and reliability of the electricity grid [18]. The latter entails lowering peak load in power use, which helps prevent dependency on expensive peak generating systems such as fossil fuel plants. Better forecasting and more controllable energy grid operations may be achieved by using DPS techniques, resulting in greater dependability and safety of power supply for customers. Furthermore, electricity providers frequently offer financial incentives to encourage consumers to reduce peak demands. Several DPS methodologies have been offered in the literature to demonstrate successful load reduction measures [19].

1.1.3 Limit grid injection

Grid-connected renewable energy systems expand their reliability ensuring the power absorption from the electricity grid in periods of low production and when the BESS has low levels of State of Charge (SOC), being unable to fulfill the demand. In the other hand, the grid-connected energy systems is also helpful in cases of high production and high levels of SOC, when battery is unable to store the surplus energy, allowing prosumers to enter the electricity market and sell the excess of energy, and increase their yearly revenue fulfilling the initial investment. Figure 1.5 reflects the linked behavior between SC, SS and grid injection.

Limits on grid injection play a pivot roll between high levels of SC and SS. The first one will get high rates avoiding as much as possible the reliance on the grid and fomenting the consumption from the local generators. However, the latter (SS) takes advantage of higher levels of grid capacity, due to economic revenues the installed generation capacity can be higher, fulfilling the total demand and economic constraints. Therefore, it is an ambiguous limitation that depends on the economical and infrastructural scenarios. Figure 1.6 reflects the linked behavior between Net present value (NPV), SS and grid injection.

Moreover, Limiting the injection of excess energy can help address grid constraints and stability issues that may arise from the intermittent nature of RES. By aligning energy production with local demand and avoiding excessive injections, grid operators can maintain a stable and reliable power supply [20].

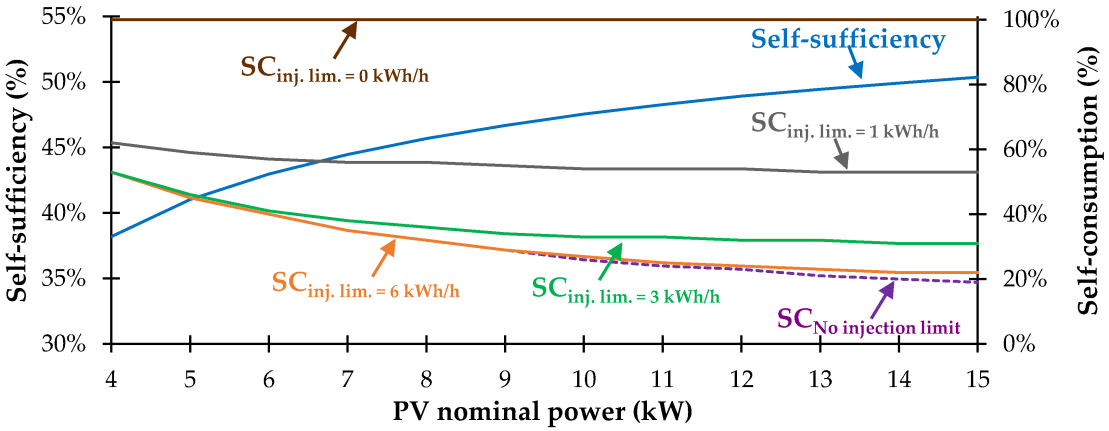

Figure 1.5: SC andd SS as functions of PV nominal power with different injection limits. [14]

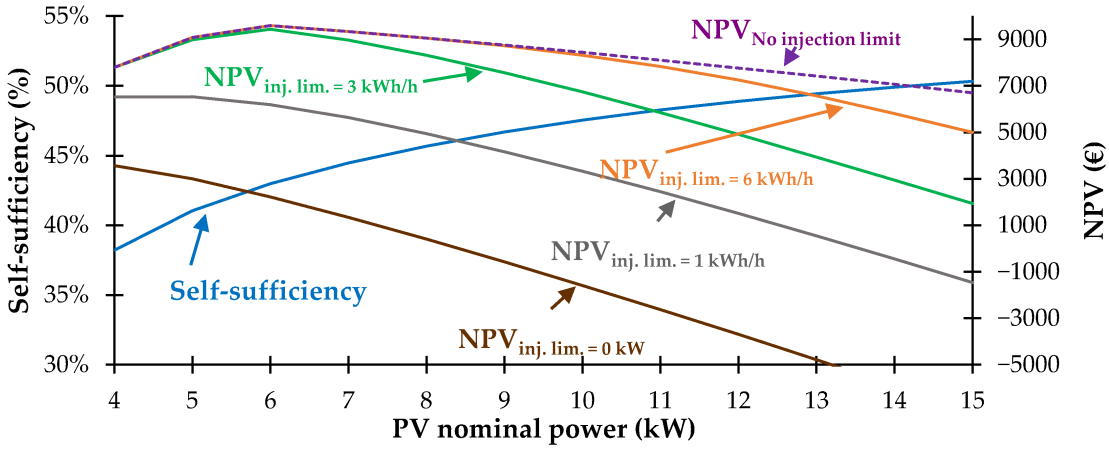

Figure 1.6: SS and NPV as functions of PV nominal power with different power injection [14]

1.1.4 Promote distributed generation

In the emerging energy market, new players are entering the scene, including prosumers, which play a crucial role in the transition towards a more decentralized energy system. Distributed energy resources (DERs) refer to the various decentralized sources of energy, including rooftop solar, small wind turbines, energy storage systems, and even electric vehicles. These resources are typically located close to the point of consumption, promoting local energy production and self-sufficiency. DERs offer benefits such as reduced transmission losses, enhanced grid resilience,

and increased renewable energy integration.

By promoting DERs individuals and communities actively can participate in the energy market to influence towards a more sustainable and cosumer-centric energy system. Therefore, the reliance on the grid reduces as local generation is predominated, in this sense SC and SS increse.

Another remarkable point is that island for example can also act as DERs at a regional level. Island generally do not have high energy consumption but possess high rate of renewable resources, once the limit of grid connection to the mainland is overcome island can perfectly give flexibility to the grid. Islands can operate interconnected to form microgirds, allowing them to operate independently or in coordination with the mainland grid.

1.1.5 Support optimal planning

Emphasizing the importance of optimal planning in the renewable energy sector, including comprehensive resource assessments, strategic location selection, and efficient project development and deployment. Optimal planning ensures the effective utilization of available resources and maximizes the benefits of renewable energy investments. In the emerging energy transition market, decision-makers face the challenge of addressing not only the system's cost but also its energy efficiency, environmental impact, and a wide range of variables that are crucial in tackling the energy and climate crisis of the 21st century [21]. To navigate this complex landscape, decision-makers require technological support to facilitate informed decision-making.

Optimal planning of renewable energy systems becomes essential in this context, as it enables decision-makers to forecast and anticipate the most appropriate pathways to pursue. By leveraging advanced technologies and data-driven analysis, decision-makers can gain valuable insights and predictions. This ensures that the chosen pathways align with the goals of energy transition, climate mitigation, and sustainable development. Therefore, Multi-criteria analysis offers a valuable technical-scientific tool for decision-making in the renewable energy sector, providing a transparent and consistent justification for the choices made [22].

Even though only a singular energy indicator is being address in this section, the maximization of SS is a criterion that encompasses several interconnected aspects. SS, as a metric, represents the ability of an energy system to meet its energy demands from internal renewable energy sources. However, by maximizing

it, decision-makers indirectly prioritize factors such as increasing the utilization of RES, optimizing BESS, and reducing reliance on external energy sources. This criterion encapsulates the broader objective of promoting sustainability, reducing dependence on fossil fuels, and mitigating environmental impact.

The motivation behind this thesis was to develop a tool that combines high-level optimization techniques with powerful open-source software. The aim was to create a user-friendly and intuitive tool that can effectively assist decision-makers in creating energy scenarios aligned with sustainability goals and energy reliability objectives. At the core of this tool lies the maximization of SS as a fundamental principle guiding the decision-making process. By leveraging optimization techniques and open-source software, the tool enables decision-makers to explore and analyze various energy scenarios. It provides them with the capability to assess different combinations of renewable energy sources, storage systems, and consumption patterns. The focus on maximizing SS ensures that the created scenarios prioritize self-reliance and reduce dependence on external energy sources.

Chapter 2

Photovoltaic, wind turbine, electrochemical storage and converter technologies

textcomp

The global energy landscape is undergoing a rapid transformation towards sustainability and efficiency, with renewable energy sources and energy storage technologies playing a vital role. Photovoltaic (PV) and wind technologies, along with electrochemical storage systems, offer significant potential for clean and reliable power generation. However, effectively integrating these technologies into existing energy infrastructures requires careful planning and decision-making. This section presents a theoretical background tailoring PV, wind, and electrochemical storage technologies, highlighting their fundamental principles and applications.

2.1 Photovoltaic technology

Irradiance (G) represents the total power received per unit area from a radiant source, measured in watts per square meter. The Sun, behaving like an ideal radiation emitter at approximately 5800 K, emits electromagnetic radiation with a spectral distribution ranging from ultraviolet to infrared, peaking in the visible range at a wavelength of approximately 0.5 μm. When solar radiation enters the Earth's atmosphere, some of the energy is dispersed, reflected in space, or absorbed

by various substances such as clouds, carbon dioxide, ozone, and air molecules. The integral of the solar spectrum over wavelength, on a surface perpendicular to the incident beam, is known as solar irradiance.

Direct irradiance (Gb) refers to the solar radiation that reaches the Earth's surface without being scattered or reflected. On a clear summer day at sea level, the direct beam irradiance is approximately 1000 W/m2. Diffuse radiation (Gd) represents sunlight that is scattered in the atmosphere but still reaches the Earth's surface. The proportion of direct and diffuse components depends on weather conditions, with diffuse radiation constituting around 20% of the total under clear sky conditions. A small fraction of the solar irradiance, called albedo (Ga), reaches a receiver on an inclined surface after reflection from the Earth's surface. The reflection coefficient (ρ) is the ratio of the radiation reflected from a surface to the radiation incident upon it. The value of ρ varies with the color of light and the nature of the reflecting surface, being highest on snow, for example. The total irradiance reaching a terrestrial receiver is the sum of the direct, diffuse, and albedo components, known as global irradiance (Gg).

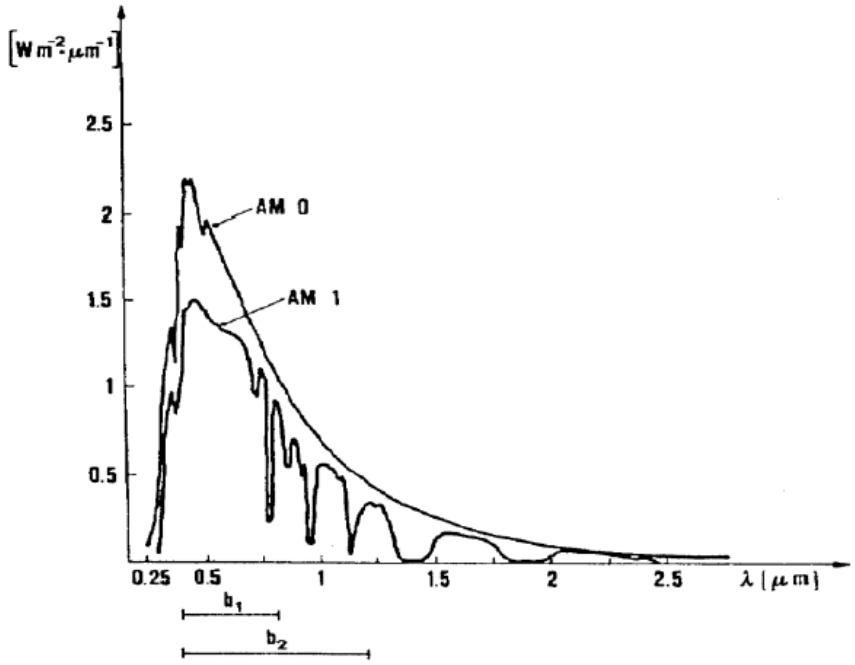

Figure 2.1: Spectral distribution of solar radiation

The intensity of solar radiation reaching the Earth fluctuates significantly due to daily and annual variations caused by the apparent motion of the Sun and irregular changes driven by weather conditions. Therefore, designing a photovoltaic system

requires accurate meteorological data specific to the installation site, considering factors such as altitude and the angle of the receiving surface. A commonly used value for solar spectrum on the Earth's surface is AM = 1.5. This value, combined with a global irradiance of 1000 W/m2 (available at noon from March to September), is utilized for qualifying photovoltaic cells and modules, with crystalline and amorphous silicon being the prevalent technologies.

2.1.1 Equivalent circuit of a PV cell

At the external terminals of a solar cell, its electrical behavior can be approximately described as an ideal current source proportional to the irradiance, in parallel with an anti-parallel diode. The equivalent circuit in Figure 2.2 provides a more accurate description of a real cell, incorporating two additional dissipative elements: a shunt resistor connected in parallel (Rsh) and a series resistor (Rs). The shunt resistance (Rsh) accounts for leakage paths along the side surfaces between the front grid and the solar cell plate. During the cell manufacturing process, efforts are made to insulate these surfaces as much as possible. The series resistance (Rs) is the sum of the semiconductor's bulk resistance, electrode resistances, and contact resistances. In practice, the primary contribution comes from the grid-shaped front electrode.

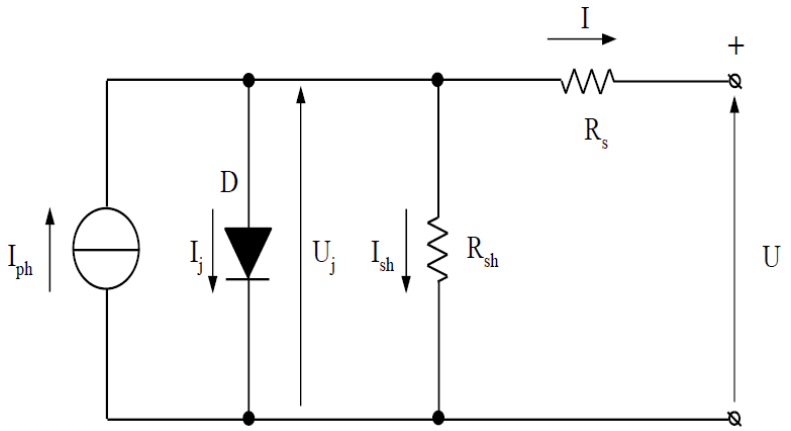

Figure 2.2: Equivalent circuit of a PV cell

The following equations are written by applying Kirchhoff's voltage and current laws to the equivalent circuit of a solar cell.

$$I = I_{ph} - I_j - U_j/R_{sh} \quad U = U_j - R_s \cdot I \tag{2.1}$$

Where U is the voltage across the load terminals and I is the current flowing through the load. The equivalent circuit is defined by the following five independent parameters: Iph, I0, m, Rs, Rsh

$$U = \frac{mkT}{q} \cdot \ln(\frac{I_{ph} - I(1 + R_s/R_{sh}) - U/R_{sh} + I_o}{I_o}) - R_s I \tag{2.2}$$

Assuming constant irradiance and temperature, it is possible to define the I-V curve, where the coordinates of its points represent the power P = U * I delivered to the load. There always exists a point PM (UM, IM), intermediate between the short-circuit conditions (0, ISC) and open-circuit conditions (VOC, 0), at which the power output of the photovoltaic cell is maximum.

2.1.2 Dependency on irradiance and temperature

The current-voltage characteristic I(U) of the solar cell, at a constant temperature T_{PV}, changes depending on the irradiance G. When G decreases, the short-circuit current I_{sc} decreases proportionally, while the open-circuit voltage U_{OC} decreases logarithmically. Figure 2.3 shows the dependency of I(U) on G and highlights the location of the maximum power points PM at $T_{PV} = 25°C$. In fact, U_{OC} remains nearly constant over a wide range of G. Only for low values of G (less than 50 W/m^2), it decreases abruptly.

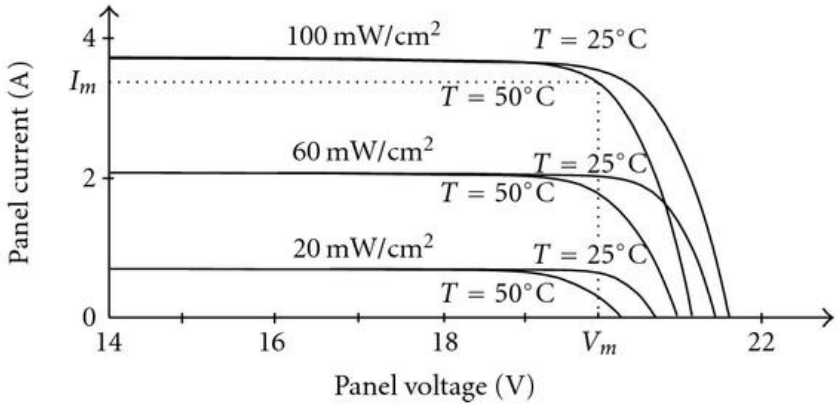

Figure 2.3: I(U) graph of a PV generator with respect to irradiance

2.1.3 Principal parameters of PV module

The solar cells within the module are typically made of semiconductor materials, such as silicon, which generate an electric current when exposed to sunlight. PV modules come in various sizes and power ratings, with larger modules capable of producing higher amounts of electricity.

The overall conversion efficiency of photovoltaic (PV) modules is determined under standard test conditions (STC), which include an irradiance of 1000 W/m², air mass (AM) of 1.5, and cell temperature (Tpv) of 25°C. The module efficiency can vary between 7% and 23% depending on the type of solar cell used. To simulate the AM 1.5 solar spectrum, specialized flash lamps are employed. These conditions replicate typical spring and autumn environmental parameters. PV modules are characterized by their peak power (Wp), which represents the maximum power output under STC. Typical Wp values range from 10 Wp to 350 Wp. Additional electrical parameters defined under STC include the short-circuit current (Isc), open-circuit voltage (Voc), current at maximum power (Im), and voltage at maximum power (Vm). Since the STC test conditions are artificially created in a laboratory, another significant parameter called the Normal Operating Cell Temperature (NOCT) is defined. The module manufacturer provides this parameter, which represents the temperature at thermal equilibrium under specific conditions: operating at open circuit with an ambient temperature (Ta) of 20°C, wind speed of 1 m/s, and irradiance of 800 W/m^2. NOCT typically ranges from 42°C to 50°C and helps estimate the cell temperature under different operating conditions. By assuming a linear dependence between the temperature difference of Tpv and Ta and the irradiance G, the cell temperature is calculated using Equation:

$$T_{pv} = T_a + \frac{NOCT - 20°C}{800W/m^2} \cdot G$$

The I(U) characteristic of an entire PV module exhibits similar trends to that of the individual cells, with an increase in voltage scale for cells connected in series and an increase in current scale for strings connected in parallel.

The energy production of a PV system is directly proportional to the solar radiation on the surface of the PV generator in kWh/m^2, and the proportionality factors are the surface area Sn of the PV generator and the conversion efficiency η_{STC}. The equation for energy production is given as:

$$E_{ac} = Hg * S_{PV} * \eta_{STC} = heq * Ppeak$$

The unit cost of modules (€/kW_p) is expressed in terms of the nominal power P_p and includes both of the aforementioned parameters. Since the nominal power of a PV generator is defined at a reference irradiance GSTC, dividing the daily radiation (in kWh/m²) by the irradiance of 1 kW/m² gives dimensionally the number of hours, per day, of operation at the nominal power of the PV field (heq). This virtual duration is defined as the "number of equivalent hours" at the reference irradiance. The product of the nominal power of the PV generator and the daily equivalent hours gives the PV energy produced in one day. This is a theoretical value that does not take into account losses: the ratio between the actually produced energy and this theoretical value defines the "Performance Ratio" (PR), which varies for each PV system.

For example, grid-connected PV systems have an average PR ranging from 0.7-0.8, while stand-alone PV systems with batteries have a PR ranging from 0.55 to 0.65.

2.2 Wind turbine technology

Wind technology is a key player in the renewable energy sector, harnessing the power of wind to generate electricity. By capturing the kinetic energy of moving air masses, wind turbines from its rotor blades can convert it into a clean and sustainable source of power, from the hub rotation due to aerodynamic forces. This rotational motion is then converted into electrical energy through a generator housed within the turbine in a structure called the nacelle [23]. In figure 2.4 is depicted the general Wind turbine components. The main ones are listed:

- Rotor Blades: The rotor blades are aerodynamically designed to capture the energy from the wind. They spin as the wind blows, converting the wind's kinetic energy into rotational energy.

- Gearbox: The gearbox is responsible for increasing the rotational speed of the rotor blades to a level suitable for electricity generation. It connects the low-speed shaft from the rotor hub to the high-speed shaft connected to the generator.

- Generator: The generator converts the mechanical energy from the rotating shaft into electrical energy. Typically, wind turbines use synchronous or asynchronous generators to produce electricity.

- Control System: The control system monitors and manages the wind turbine's operation. It adjusts the orientation of the rotor blades to optimize their alignment with the wind direction. The control system also regulates the speed of the turbine and manages safety features.

In Figure 2.5 is consider the stream tub that models the turbine interaction with the wind. Rotational speed an the wind speed are fundamental to regulate performance, this balance is known as the tip speed ratio (λ) in equation 2.3. Additionally, another factor under consideration is the angle of attack (α) in which the wind hits the chord line of the blades.

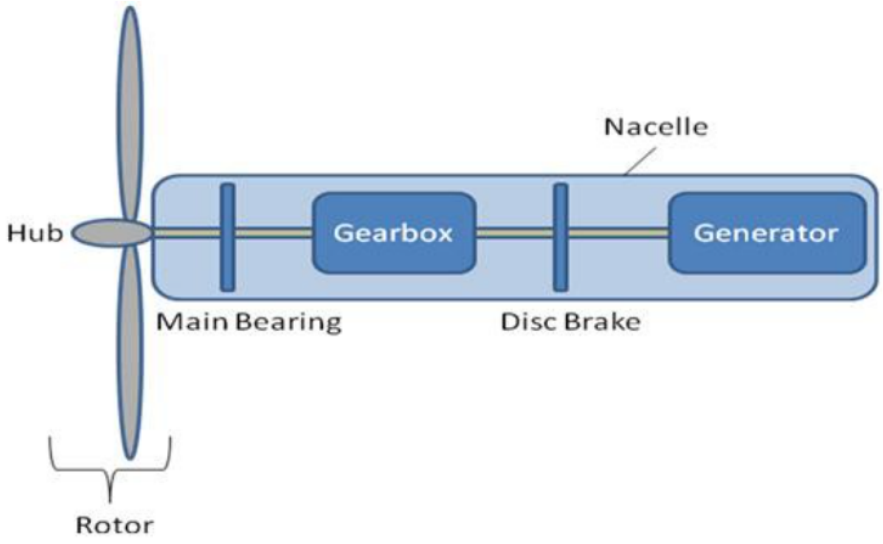

Figure 2.4: Main components of a wind turbine.[23]

$$\lambda = \frac{2\pi f r}{u_1} \tag{2.3}$$

Where f is the blades frequency of rotation (Hz) and r is the blade length (m). The power coefficient is the efficiency of power generation of a wind turbine and varies from each type, it is represented as the ratio between mechanichal power P_{mec} generated by the blades and the wind power at constant speed U, which can also be as the ratio of real generated power and ideal power. The power coefficient can also be expressed in function of tip speed ratio and angle of attack, maximum value of 0.59 known as the Betz limit $C_p(\lambda, \alpha)$ [23].

Finally, the usable power from the wind speed is represented as in equation 2.4. Nonetheless, each type of wind turbine has its own representing power curve

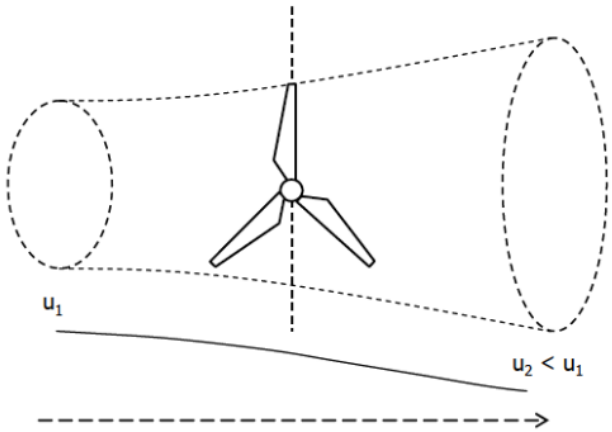

Figure 2.5: Wind speed profiles along the stream tub.[3]

representing their phases of operation. in Figure 2.6is shown an ideal wind turbine power curve, the cut-in and cut-out wind velocities are the operational limits of the turbine, these two thresholds ensure the minimum operation point to activate the rotor and the latter avoid structural damage.

$$P = \frac{1}{2} C_p(\lambda, \alpha) \rho_{air} A_T u_1^3 \tag{2.4}$$

In terms of electromechanical conversion technology, the market is divided between two types of turbines [3]:

- Fixed-speed turbines (40% market share)
- Variable-speed turbines (60% market share), which are a more recent development. These turbines are equipped with either Doubly Fed Induction Generators (DFIG, accounting for 45% of the market) or Permanent Magnet Synchronous Generators (PMSG, accounting for 15% of the market).

The main characteristics of wind are its intensity and direction. Anemometers are used to measure these parameters, typically placed at a height of around 10-15 m above the ground. To utilize experimental wind data, it is necessary to adjust them to the hub height of the wind turbine, as wind speed depends on the height and the type of terrain. This adjustment is done using the concept of roughness, represented by the parameter Z_0, which quantifies the terrain's roughness. The formula used for this adjustment is as follows:

$$U(h, z_0) = U(h_{ref}) \cdot \left(\frac{\ln\left(\frac{h}{z_0}\right)}{\ln\left(\frac{h_{ref}}{z_0}\right)} \right)$$

The wind speed increases with height up to 100 m. The lowest roughness values correspond to flat surfaces such as beaches and seas, while the highest values are found in cities with tall buildings and skyscrapers.

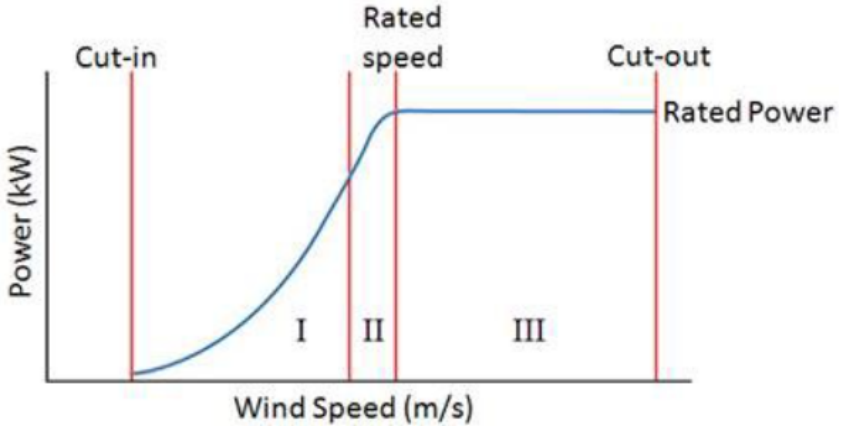

Figure 2.6: Ideal wind turbine power curve[23]

Appropriate sites for hosting wind farms should have an average wind speed of at least 5 m/s. From a statistical perspective, it is necessary to calculate the number of hours during which the wind speed falls within a certain range for a given wind direction. This involves grouping the data into velocity classes and calculating the mean value and standard deviation. The resulting wind rose graph illustrates the prevailing wind directions, indicating the optimal orientations for wind turbines.

This statistical analysis is crucial for wind turbines because their conversion efficiency varies significantly with wind speed, unlike photovoltaic generators whose efficiency remains relatively constant with solar irradiance.

In order to perform the calculation of energy production, it is required simultaneous knowledge of:

- The distribution of wind speed frequencies, often represented by the Weibull distribution fw(U). Which gives the probability of a wind speed U occurring at a specific location.

- The power curve Pel(U) which represents the electrical power output as a function of wind speed, which represents the relationship between the wind speed (U) and the electrical power output (Pel) of a wind turbine.

Productivity is the sum of the products, for each wind speed at hub height, of the power curve and the distribution of wind speed frequencies. The profitable wind speed range is (3-25) m/s, and the calculation of energy production and grid injection is performed over a one-year period (8760 hours), as summarized in the equation:

$$E_{AC,\text{wind,year}}(kWh) = 8760 \cdot \sum_{U=4m/s}^{U=25m/s} (P_{el}(U) \cdot f_W(U))$$

2.3 Electrochemical Storage technology

In this section electrochemical batteries are introduce, explaining their principal fundamentals and essential parameter that characterized them. In the emerging energy systems batteries are fundamental to address the intermittency issue, even though energy storage is dominated by pumped hydro, batteries are recognized for high-value opportunities helping energy transition by managing peak demands, increasing grid reliability and allow the smooth penetration of RES. Sodium-sulfur batteries are available in the market for applications in the grid, and Lithium-ion batteries are commonly found in commercial electronics and implemented for grid storage in electric vehicles, with vehicle-to-grid (V2G) approaches [24].

Regardless the chemistry of electrical batteries, all of them store energy through the electrode composition within charge transfer reactions. Inside the plenty Electrical Energy Storage (EES) technologies, they vary in application due to their characteristics and strategies. Categories for applications such as power quality, load shifting, bulk power management are in function of the discharge time at rated power and the installed capacity of each different technology. For instance Supercapacitors are applied for power quality solutions due to their higher power and more expanded cycle life than batteries. In table 2.1 are listed different types of batteries with their respective characteristics, highlighting even maturity, duration and costs.

Batteries are defined as parallel or series connected cells providing the desired voltage and capacity. A cell has a negative and positive electrode, where the redox

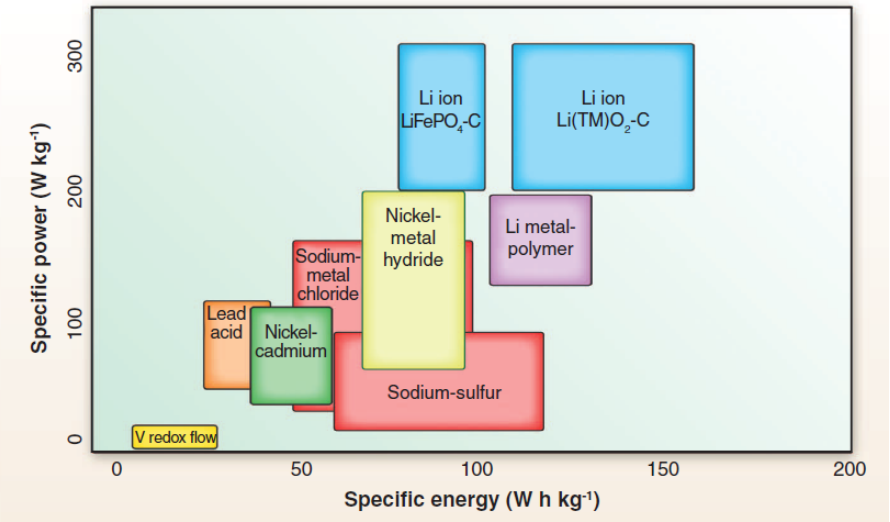

Figure 2.7: Gravimetric power and energy densities for different rechargeable batteries [24]

reactions take place and they are separated by an electrolyte. Once both terminals are connected from outside the chemical reactions begin at both electrodes, thus liberating electrons and providing current [24].

Figure 2.7 depicts the most common rechargeable batteries, their energy and power storage properties, providing complementary information to table 2.1. As noticed Lithium ion batteries (LIB) technologies outcome its competitors in terms of capacity and providing high specific power. They are characterized by low molecular weight, small ionic radius and low redox potentials, the latter explains why they can provide high-output voltage and high-energy densities. furthermore, their long cycle life and rate capability out-stand LIB to portable electronics market and nowadays for the integration in electric vehicles, which will turn in expanding the electrical grid flexibility with V2G approaches.

In this research study is chosen Lithium-ion technology as EES, it has been motivated due to the fact realated to its superior specific power, high energy efficiency, and environmentally friendly nature compared to other technologies like lead-acid batteries. Lithium-ion batteries exhibit reduced self-discharge and do not require high operating temperatures. These advantageous characteristics have made them the preferred choice for electric vehicles and have contributed to significant research investments in this field. Furthermore, the decreasing installation costs, ranging from approximately 700 €/kWh for domestic users to 300 €/kWh for large-scale installations, coupled with expected improvements in

cost and performance, indicate a promising future for Lithium-ion technology in both mobile and stationary applications [24].

Table 2.1: Technology Option Maturity. Adapted from [24]

Technology	Capacity (MWh)	Power (MW)	Duration (hours)	% Efficiency (total cycles)	Cost ($/kWh)
Advance Pb-acid	3.2–48	1–12	3.2–4	75/90 (4500)	625–1150
Na/S	7.2	1	7.2	75 (4500)	445–555
Zn/Br flow	5–50	1–10	5	60/65 (>10000)	340 –1350
Fe/Cr flow	4	1	4	75 (>10000)	300–400
Zn/air	5.4	1	5.4	75 (4500)	325–350
Li-ion	4–24	1–10	2–4	90/94 (4500)	90–1700

Chapter 3

Optimal configuration for renewable exploration

This chapter describes the mathematical models that represent an energy system with electricity as its only energy carrier, and the power sharing between its components. The generation production is supplied by RES, specially PV panels and wind turbines. Storage is performed by BESS with a centralized approach, and the DC/AC inverter allows unidirectional flow within the electricity grid and loads. As an starting point these models were adopted from [3] and [25]. However, This thesis work introduces a different approach for power flow management. Through a process of linearization, the original quadratic and polynomial representations were successfully reformulated into a total linearized form. This transformation enables the system to converge more rapidly towards an optimal solution. Moreover, operational logic of BESS and power exchange within the electrical network are incorporated inside the optimization problem's constraints. The chapter begins by explaining the mathematical models of RES generation, BESS, Electronic converter and economic. Then, concluding with the optimization techniques utilized for both single-site and multiple-site scenarios.

3.1 Energy Balance Model

The energy balance model represents the power sharing between generators, load, grid and energy storage in an hourly basis. Within the model, the grid is integrated to depict the hourly energy exchange, including injection and absorption, within

the energy system for single-site scenarios. Additionally, it enables the analysis of energy exchanges between different regions in the case of multiple-site scenarios. By incorporating the grid functionality, the model facilitates a comprehensive understanding of energy flows and interactions at both the individual site and regional levels, enhancing the overall analysis of the energy system.

The modelled energy system is represented in Figure 3.1. The main components are: PV generators, wind turbines, electrochemical batteries, electronic converters, electric grid and loads. The system's core is the DC bus, connecting all renewable sources to the battery voltage. Loads are in AC and can be powered by the grid when renewables are unavailable. A unidirectional inverter supplies AC power to the loads, sized based on the combined capacity of photovoltaic and wind generation, the BESS is not included in this sizing process. The implementation of energy storage addresses the intermittent nature of renewable generation, thereby maximizing self-sufficiency.

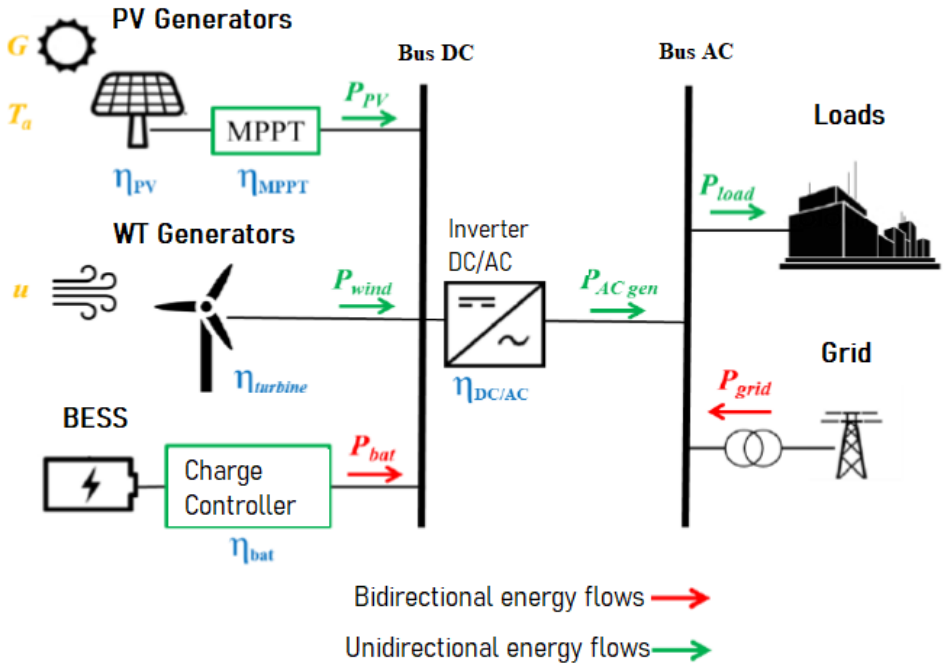

Figure 3.1: Hybrid energy system connected to the grid consisting of photovoltaic and wind generators with energy storage. [3]

3.1.1 Photovoltaic production model

The generation consists of PV panels and wind turbines both have a consolidated Technology Readiness Level of 11 (TRL 11) and continually are addressed to improvement [26]. Regarding the PV production simulation, it is evaluated following the model described in [27].

The power absorbed by the DC/AC inverters is derived from real irradiance profiles obtained by PVGIS database. specific orientation of PV generators are settled based on the desired location to be simulated, usually the types of PV modules are set as fixed-axis and tracking. In equation 3.1 is represented the DC power the solar panel produce, its nomimal power (P_{nom}^{PV}) is multiplied by the hourly horizontal irradiance ($G(t)$) which lower limit is ($G_0 = 0.0177\frac{kW}{m^2}$) to avoid malfunctioning of the inverter, defines the minimum value to turn on the inverter. The standard test conditions are ($G_{STC} = 1\frac{kW}{m^2}$ and $T_{STC} = 25°C$), at which the rated peak power for all commercial PV modules is measured [3].

$$P_{DC}^{PV}(t) = P_{nom}^{PV} \cdot \frac{G(t) - G_0}{G_{STC}} \cdot \eta_{therm}\eta_{mix} \tag{3.1}$$

$$\eta_{mix} = \eta_{dirt} \cdot \eta_{reflection} \cdot \eta_{mismatch} \cdot \eta_{cable} \tag{3.2}$$

The losses due to cell temperature are represented in equations 3.4 where ($\gamma = 0.3 \div 0.5\frac{\%}{°C}$) is the power reduction coefficient, in this work is used a $0.5\%/°C$ value. The PVGIS API provides the hourly air temperature in Celsius ($T_a(t)$) of the analyzed region [28]. The losses due DC cables, to reflection and dirt of PV module's glass, and tolerance and $I - U$ mismatch, are globally $\approx 8\%$ [29], then the miscellaneous efficiency is approximately $\eta_{mix} \approx 92\%$. In equation 3.3 NOCT is generally the normal cell operating temperature written in the PV module data sheet. In this work it corresponds to a typical value $NOCT = 45°C$ and G_{NOCT} is the solar irradiance ($800\frac{W}{m^2}$) corresponding to the NOCT conditions. In this sense the PV cell temperature can be calculated in $°C$ as represented in equation 3.3.

$$T_c(t) = T_a(t) + \frac{NOCT - 20°C}{G_{NOCT}} \cdot G(t) \tag{3.3}$$

$$\eta_{therm} = 1 - \gamma(T_c - T_{STC}) \tag{3.4}$$

3.1.2 Wind Turbine production model

In the other hand, for wind power simulation the link between wind speed and power output is nonlinear. Under steady-state conditions, the mechanical power converted by a horizontal-axis wind turbine is a cubic function of wind speed and can be expressed as [23]:

$$P_{mec} = \frac{1}{2} \cdot \rho_{air} \cdot A_T \cdot u_w^3 \cdot C_p(\lambda, \alpha) \tag{3.5}$$

- $\rho_{air} \approx 1.225 \frac{kg}{m^3}$ at 15 °C and 1 atm; it is th air density.
- A_T is the cross sectional area of the rotor disk (perpendicular to wind speed), a function of blade length.
- $u_w \frac{m}{s}$ is wind speed, at height z of the rotor hub, passing through the cross sectional area.
- $C_p(\lambda, \alpha)$ is the power coefficient, i.e., the ratio of converted power to available power, and is a function of the tip-velocity ratio λ and angle of attack α.

The model of wind turbine production is performed by the empirical correlation of power curves "wind speed - AC power output", which manufactures provide on the datasheet of the specific wind turbine. Power output and wind velocities are generally provided as a discrete list of points, then a linear interpolation is performed between power and wind speed values to obtain the results of power production for a single turbine ($P_{AC}^{singl,WT}$) and the overall production for a wind farm (Equation 3.7) multiplying the number of turbines (n_{WT}).

In Figure 3.2 is represented a wind turbine power curve with $850kW$ nominal power and cut-in wind speed of $3m/s$ and a cut-out of $25m/s$. The first zone for low to medium wind speed ($4 - 9m/s$) is a cubic function; the second zone is a nearly linear function close to the rated wind speed ($10 - 14m/s$); and the third zone is a constant power output equal to the rated power output in the portion from rated wind speed to shutdown wind speed ($15 - 25m/s$) [3]. Finally, it is necessary to transfer the data to the turbine hub height using the logarithmic formula represented in equation 3.6[23], where u_{ref} is the reference wind speed, Z_o is the terrain roughness, h is the hub height and h_{ref} is the wind speed at wich the wind speed is measured. PVGIS provides hourly wind speeds at $10m$ above sea [28].

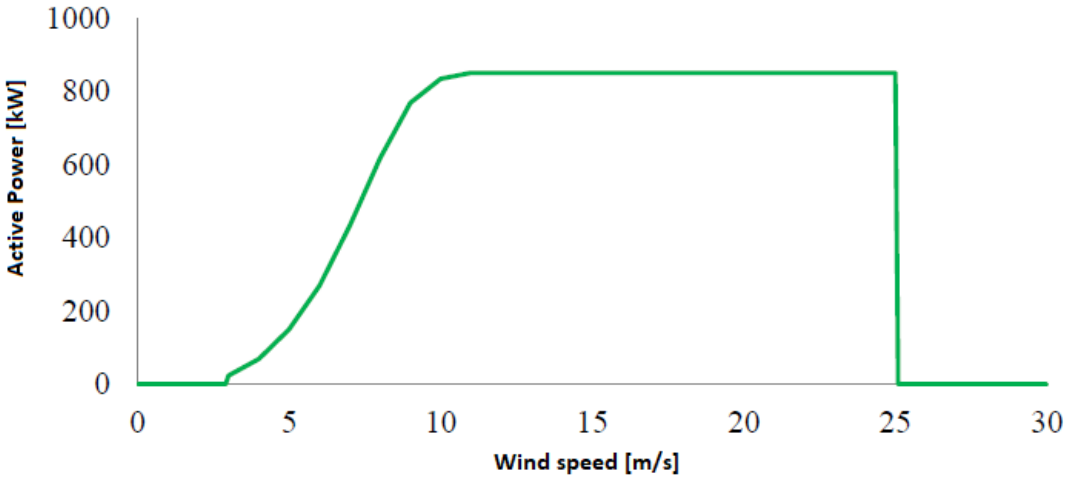

Figure 3.2: Wind Turbine general power curve correlation [3]

$$u_w(h, z_0) = u_{ref} \cdot \frac{\ln \frac{h}{z_0}}{\ln \frac{h_{ref}}{z_0}} \tag{3.6}$$

$$P_{AC}^{farm,WT} = P_{AC}^{singlWT} \cdot n_{WT} \tag{3.7}$$

3.1.3 Battery Energy Storage System model

Having an accurate storage model is crucial for evaluating energy and cash flow. There are various electrical models available, each allowing simulation of the storage system with different levels of precision. The more sophisticated models enable determination of key parameters such as State of Charge (SOC) and the number of cycles performed by the storage system, state of health (SOH) [30] [31].

The SOC, calculated on an hourly basis and compared to the limits (SOC_{min} and SOC_{max}), is used to estimate the amount of energy stored or that can be stored in the battery with a nominal capacity (C_s). Instead the SOH is implemented in the model in order to know life time of the BESS, generally 8 years (3500 cycles) [3].

The model of the battery takes as input specific parameters represented in Table 3.1, for commercial storage in PV applications, to simulate the behavior of the storage system over time. The $SOC(t)$ is in function in time of its previous value

$SOC(t-1)$ 3.8 and must satisfy the limits of maximum and minimum discharges to avoid battery damages as represented in equation 3.9.

$$SOC(t) = SOC(t-1) - \frac{\eta_{bat} \cdot P^b(t-1)}{V_{b,r} \cdot C^s} \tag{3.8}$$

$$SOC_{min} \leq SOC(t) \leq SOC_{max} \tag{3.9}$$

Table 3.1: Specifications of a Li-ion Battery element [32]

Battery rated capacity	(C^S)	100 Ah
Battery rated voltage	$(V_{b,r})$	12 V
Lifetime (cycles)	(N_{cycles})	3500
Lifetime (years)		8
Maximum power	(P^b_{max})	≈2.4 kW
Charge-discharge efficiency	(η_{bat})	0.88

3.1.4 Electronic Converter Model

The interaction with the the grid (AC side) is performed by the DC/AC converter, which mages the power output from wind, PV and storage. The resulting power after the inversion process is obtained from the inverter efficiency η_{inv} taking into account the DC/AC losses. In equation 3.10 is defined as the ratio of AC power delivered to the grid and DC power input.

$$\eta_{inv} = \frac{P_{AC}}{PDC} = \frac{P_{AC}}{P_{AC} + P^{glob}_{loss}} \tag{3.10}$$

Where P^{glob}_{loss} stands for the inverter global losses, defined in [33].

$$P^{glob}_{loss} = P_0 + C_L \cdot P_{AC} + C_Q \cdot P^2_{AC} \tag{3.11}$$

C_L is the linear loss coefficient (due to the conduction of diodes, IGBT and switching losses), P_0 are the no-load power losses along the operation (due to the supply of auxiliary circuits, and C_Q is the quadratic loss coefficient (due to the conduction of MOSFETs and the resistive contribution). The sizing of inverters is in function of nominal power genration from RES.

3.2 Financial Model

In order to evaluate the financial viability of energy system investment or project, a widely use method of financial model incorporates Net Present Value (NPV) and Internal Rate of Return (IRR). Over a specified time period NPV is a financial indicator to determine the profitability of an investment, taking into account the cash inflows and outflows. At the end of the project lifetime positive NPV values means a profitable investment, instead negative values represent a potential loss.

$$\text{NPV} = -C^I - \sum_{t=1}^{T} \frac{C_t}{(1+r)^t} + \sum_{t=1}^{T} \frac{R_t}{(1+r)^t} \tag{3.12}$$

NPV is expressed in equation 3.12 [14], where C^I is the initial cost of investment, r is the discount rate, C is the absolute value of negative cash-flows year and R is the positive cash-flows.

On the other hand, IRR is a financial metric employed to measure the profitability of an investment. It represents the discount rate at which the NPV becomes zero. A higher IRR indicates a more appealing investment opportunity. It is represented in 3.13 where CF_t is the total of cash-flows.

$$NPV = \sum_{t=0}^{T} \frac{CF_t}{(1+IRR)^t} = 0 \tag{3.13}$$

The negative cash-flows of an energy system project include the cost of operation and maintenance (O&M), including the replacement of batteries, possible damages in the RES generation and buying electricity from the grid. The positive ones include the earnings due to energy injection to the grid and the monetary savings due to self production, avoiding buying electricity from the grid.

Investors and decision-makers obtain significant insights into the financial viability and prospective returns of an investment by combining NPV and IRR. This

allows them to evaluate the feasibility of a investment project.

By utilizing NPV and IRR together, investors and decision-makers gain valuable insights into the financial feasibility and potential returns of an investment. This enables them to assess the desirability and financial attractiveness of projects, facilitating well-informed investment decisions.

3.3 Optimization Model

Single-objective optimization problems focus on the challenge of optimizing a single objective, which can involve either maximizing or minimizing it. These problems involve decision variables, which are the variables that can be adjusted or chosen to achieve the optimal solution. The decision variables are subject to a set of constraints, which are conditions or limitations that must be satisfied. These constraints help shape the feasible region, which represents the range of valid solutions. The ultimate goal in single-objective optimization is to find the best possible solution within the given constraints, maximizing or minimizing the objective function to achieve the desired outcome [34].

The optimization problems discussed in this chapter face a significant challenge when dealing with large sets of decision variables and constraints. The presence of a large number of variables and constraints can make it challenging to find a feasible solution that satisfies all the requirements. While single-objective quadratic and linear optimization problems are mathematically well-behaved and do not inherently struggle with convergence, their implementation within solvers can sometimes lead to convergence issues. These implementation-related challenges will be further elucidated in the subsequent chapter. This chapter instead, presents a comprehensive analysis of single-objective optimization problems for energy systems with electricity as their only energy carrier, considering two different configurations: the single-site approach and the multiple-site approach. The chapter provides a detailed description and examination of the analysis conducted for these optimization problems.

3.3.1 Single-site optimization model

The single-site optimization model is implemented to maximize self-sufficiency while ensuring compliance with power balance and economic constraints. The outcome of the optimization model determines the optimal configuration of the energy system

that maximizes the utilization of renewable energy sources and minimizes reliance on external power supply. The first step is to define the objective in function of the decision variable, in equation 3.14 is represented in fucntion of (n^{PV}, n^{WT}, C^s) which are the number of PV panels, Wind Turbines and storage capacity. C_t^{PV} and C_t^{WT} represent the production of PV panels and wind turbines for the t^{th} hour. The P_t^d and P_t^b are the power demand and dicharge or charge power battery.

$$SS = \sum_{t=1}^{T} \frac{n^{PV} \cdot C_t^{PV} + n^{WT} \cdot C_t^{WT} + P_t^b}{P_t^d + P_t^b} \tag{3.14}$$

As it can be noticed the objective equation is not linear, meaning a significant increase in the complexity of solving the optimization problem. However, after conducting the analysis, it was determined that the entire model could be linearized. This involved transforming the original problem from a mixed-integer quadratic formulation to a mixed-integer linear formulation. Starting from the objective function, it was deduced that maximizing self-sufficiency is equivalent to minimizing the power absorption from the grid.

$$\text{Maximize} \quad SS \quad \equiv \quad \text{Minimize} \quad \sum_{t}^{T} P_{abs}(t) \tag{3.15}$$

The primary goal of the model is to achieve a high level of self-sufficiency, where the energy generated from renewable sources within the system meets a significant portion of the overall energy demand. To accomplish this, the model considers various factors such as the maximum potential capacity of renewable energy technologies, the resource availability, and the demand forecast for each region. Additionaly, as previously mentioned the model needs to meet power balance, financial and battery constraints.

As represented in the following optimization problem, the linear objective is the maximization of P_{abs}, per convention $P_{abs}(t) \in \mathbb{R}^-$, meaning that the maximization will bring the objective as close as possible to zero. The power balance in the system is achieved by managing the generation from renewable sources, the energy storage management, and the grid interaction. The generated power from renewables is the sum of the power produced by PV panels and wind turbines, as seen in equation 3.16.

$$P^G(t) = n^{PV} \cdot C^{PV}(t) + n^{WT} \cdot C^{WT}(t) \tag{3.16}$$

The decision variables, represented by n^{PV} and n^{WT}, indicate the optimal number of PV panels and wind turbines, respectively. The installed capacity of each PV

panel is fixed at $1MW$, while each wind turbine has a capacity of $2MW$. Then, the hourly energy generation will depend on the available energy resources in the analyzed area, represented by $C^{PV}(t)$ and $C^{WT}(t)$. The storage management depends on BESS capabilities and the hourly need to charge or discharge the batteries, per convention ($P^b < 0 \quad discharging$) and ($P^b > 0 \quad charging$). Reciprocally, the interaction with the grid works basically the same with the goal to fulfill energy demand the absorption power must be negative ($P_{abs}(t) \in \mathbb{R}^-$) and the injection power positive ($P_{inj}(t) \in \mathbb{R}^+$).

$$\begin{aligned}
&\text{Maximize:} \quad \sum_{t}^{T} P_{abs}(t) \\
&\text{Subject to:} \\
&Power \quad balance: \\
&\qquad P^G(t) - P^d(t) - P^b(t) - P_{abs}(t) - P_{inj}(t) = 0 \\
&Financial: \\
&\qquad NPV \geq 0 \\
&Battery: \\
&\qquad E^b(t) = \begin{cases} E^b(t-1) + \eta_c(1 - S(t))P^b(t), & \text{if } charging \\ E^b(t-1) + P^b(t)S(t)/\eta_d, & \text{if } discharging \end{cases} \\
&\qquad t \in \mathbb{Z}^+ \\
&\qquad S(t) \in [0,1] \\
&\qquad P_{abs}(t) \in \mathbb{R}^-
\end{aligned}$$

The NPV as represented in equation 3.12 is linear as the discount rate (r) is constant defined by the user, It is expected to be the value that makes $NPV = 0$, meaning the desired IRR. The NPV must be higher or equal than zero in order to have a positive return of the initial investment. It is remarkable to mention that the model only ensures the $NPV \geq 0$ at the end of the time simulated. This financial constraint is link to the decision variables because both initial investment and negative chasflows depend on the installed capacity of generation and storage, and the costs for operation and maintenance. As the problem is analyzed in an hourly timeframe the NPV needs to be converted from yearly to hourly basis, starting from the discount rate as equation 3.17 reprents it and the derived NPV is expressed as 3.18.

$$r_{hour} = (1 + r/365)^{(1/24))} - 1 \tag{3.17}$$

$$\text{NPV} = -C^I - \sum_{t=1}^{T} \frac{C_t}{(1 + r_{hour})^t} + \sum_{t=1}^{T} \frac{R_t}{(1 + r_{hour})^t} \tag{3.18}$$

Furthermore, the power balance constraint ensures the reliability of energy supply by balancing demand and generation. The implementation of this constraint enables the management of power flow. When combined with the other constraints, it establishes the operating rules and conditions for each component involved inside the model. As the objective function is the minimization of P_{abs}, the energy system modeled will predominate the power that has been locally produced or stored than the one absorbed from the grid. In addition, the overproduction can be either stored or injected to the grid, this will depend not only if the batteries can be recharged at time (t) but also on the capacity limitations of batteries and transmission lines. Moreover, the liked economic constraints within injection and storage capacities can also influence, as the increase in storage capacities means an increment in negative cash-flows and power injection to the grid the opposite.

BESS increases the complexity of the model but increases reliability of energy systems based on RES, hence maximizes SS. Nonetheless, E^b is defined as a mix integer quadratic function having two possible solutions to ensure charging or discharging the battery. Even though quadratic problems do not represent a hazard for convergence, it may do for computational cost and even more when modelling systems with large sets of decision variables and constraints. Accordingly, it is the case when planning energy scenarios for extended periods with high-resolution data. Therefore, linearizing the proposed optimization problem delves the path for the chapter 4 when the model will be computationally implemented.

The battery management has been modify from a SOC management approach to purely calculate the energy inside the battery and adding constraints that simulate the limits SOC management takes under consideration, as the one represented in equation 3.9. The SOC management can be formulated as:

$$SOC(t) = \begin{cases} SOC(t-1) + \eta_c(1 - S(t))P^b(t)/C^S, & \text{if } charging \\ SOC(t-1) + P^b(t)S(t)/\eta_d C^S, & \text{if } discharging \end{cases}$$

As it can be noticed, the difference between SOC and E^b calculations is the addition of C^S decision variable in case of SOC formulation. The reason why the latter

formulation has been selected is again on terms of reducing complexity, adding decision variables to the expression may be translate to more computational cost.

Therefore, the additional constraints to be implemented for E^b encompasses the initial state of energy inside the battery, which is supposed to be equal to 20% of the storage capacity ($E^b(t=0) = 0.2 \cdot C^S$). Afterwards, as previously mention, $E^b(t)$ has two possible solutions, representing when the BESS is charging or discharging. To accomplish it, the binary decision variable $S(t)$ is incorporated to the model, by convention $S(t) = 0$ when charging and $S(t) = 1$ when discharging. The parameters η_c and η_d represent the charge and discharge efficiencies that usually take values of $\approx 90\%$ each.

The implementation of the above mentioning optimization problem would require Mix-integer Quadratic Programming (MIQP) approaches. Nonetheless, the complete linearization of the model is possible by implementing linear programming methods, such as The Big M method. This technique involves introducing a large positive constant "M" to represent a huge upper/lower bound to the decision variable under analysis ($E^b(t)$) [34]. In this sense, energy inside the battery will not take values technical unfeasible but still following the charge/discharge conditions, with the help from the binary variable $S(t)$ and reformulating thee constraints, the original problem can be transformed into an equivalent Mix-integer Linear Programming (MILP) problem. It is worth mentioning that, the over sizing of M could result on suboptimal or unrealistic solutions thus, its value selection should be done judiciously. In this thesis is selected as $M = 3$ times the storage capacity C^S.

Charging:

$$E^b(t) \leq E^b(t-1) + \eta_c \cdot (1 - S(t))P^b(t) + S(t) \cdot M \cdot C^S$$
$$E^b(t) \geq E^b(t-1) + \eta_c \cdot (1 - S(t))P^b(t) - S(t) \cdot M \cdot C^S$$

Discharging:

$$E^b(t) \leq E^b(t-1) + S(t)P^b(t)/\eta_d + (1 - S(t)) \cdot M \cdot C^S$$
$$E^b(t) \geq E^b(t-1) + S(t)P^b(t)/\eta_d - (1 - S(t)) \cdot M \cdot C^S$$

3.3.2 Multiple-site optimization model

The optimization model for the multiple-site approach focuses on a single objective, which is to minimize dependence on the grid. According to the adopted convention This objective is essentially equivalent to maximizing the amount of power absorbed from the grid, particularly from the mainland. Therefore, the objective can be

defined as

$$\sum_{t}^{T} P_{abs,v}^{Mainland}(t)$$

HVDC lines that connect the region to mainland were decided to be modelled as virtual generators that can have bidirectional power flows, representing the absorption or injection from/to the grid. The subscript v indentifies the each virtual generation inside the modelled energy system, and the objective will be the minimization of reliance from mainland for each one of them. Also, inside the model will only consider medium and high voltage transmission lines, for Italy representing the 220 kV and 380 kV.

Furthermore, to uniquely identify each site within the model, a new subscript, denoted by i, will be introduced. This subscript will serve as an identifier for each individual site, allowing for differentiation and specific analysis of each site within the model. For instance the power locally generated for a site i can be identify as P_i^G. Additionally to these minor but important changes, it is introduced to the model a new constraint related to the power flow between each site inside the model. In order to linearized the power flow equations, a linear approximation is performed calculating the Power Transfer Distribution Factors (PTDF), which is a technique used in power systems analysis to determine the power flows and voltage profiles in a network. The PTDF allows to estimate the power transfer distribution across transmission lines in response to changes in generation or load. In this sense, the modeler will need to introduce the respective PTDF of the network under analysis and its lines characteristics and limits. The PTDF results will represent the sensitivity power flows (f) from bus 1 to bus n and through line 1 to line m, with respect to changes in Power network (P^N) regarding absorption or injection.

$$\text{PTDF} = \begin{bmatrix} f(1,1) & f(1,2) & \dots & f(1,n) \\ f(2,1) & f(2,2) & \dots & f(2,n) \\ \vdots & \vdots & \ddots & \vdots \\ f(m,1) & f(m,2) & \dots & f(m,n) \end{bmatrix} \begin{bmatrix} P^N(1) \\ P^N(2) \\ \vdots \\ P^N(n) \end{bmatrix}$$

$$\text{Maximize:} \quad \sum_{t}^{T} P_{abs,v}^{Mainland}(t)$$

Subject to:

$$Power \quad balance:$$

$$P_i^G(t) - P_i^d(t) - P_i^b(t) - P_{abs,i}(t) - P_{inj,i}(t) = 0$$

$$P_v^{min} \leq P_{abs,v}^{mainland}(t) \leq P_v^{max}$$

$$P_v^{min} \leq P_{inj,v}^{mainland}(t) \leq P_v^{max}$$

$$Financial:$$

$$NPV \geq 0$$

$$Network:$$

$$f_m^{min} \leq f_m(t) \leq f_m^{max}$$

$$Battery:$$

$$E_i^b(t) = \begin{cases} E_i^b(t-1) + \eta_c(1 - S(t))P_i^b(t), & \text{if } charging \\ E_i^b(t-1) + P_i^b(t)S(t)/\eta_d, & \text{if } discharging \end{cases}$$

$$t, i, m, v \in \mathbb{Z}^+$$

$$S(t) \in [0,1]$$

As it can be noticed, the network constraint contains the subscript m representing the m^{th} transmission line inside the network, which flow (f_m) must compliant with its line limits. Then the concept from single-site to multiple-site optimization model follows the same structure but the latter one adds up the consideration of power exchange between regions and mainland, at the end of the simulation the results will show the levels of self-sufficiency of the regions united as a whole. The subscripts were added to take under consideration the all the energy system. Nonetheless, the system is simplified from a realistic power system as it is only considered a DC power flow and no transformers where taken under consideration inside de model.

Chapter 4

Python-based planning and optimization tool for supporting energy transition

In this section will be described the mathematical models implementation inside the software, its architecture and approach. The program is based on the proposed framework in [3] which studies the optimal power sharing between PV panels, Wind Turbines, Electrochemical Storage and electrical grid in urban districts. Additionally, this new tool provides a user-friendly interface and incorporates advanced optimization techniques capable of handling larger sets of hourly data spanning up to 25 years, equivalent to approximately 219,000 hours. This enhanced capability allows for more comprehensive analysis and optimization of energy systems over extended time periods. The tool also includes a well-organized and automated local database management system. These capabilities are made possible through the integration of open-source modules and libraries within the Python integrated development environments.

By using the tool the user can develop energy scenarios from single to multiple locations in a hourly time-step basis, with electricity as the only energy carrier. The first dimension is focus on finding, through a linearized optimization model, the optimal values of capacities for renewable generators and BESS that achieve the maximum level of self-sufficiency, which must be compliant with economic and power balance constraints. Moreover, to model multiple regions under analysis the objective is the same but, the inclusion of the electric grid becomes essential for connecting the energy flows between these locations. By incorporating the

electric grid into the modeling framework, the tool enables the representation and analysis of energy exchange and transmission between different regions. This allows for a more comprehensive understanding of dynamics of the energy system. The optimization problem definition and their linearization are well-described in sections 3.3.1 and 3.3.2.

This chapter instead, focuses on the implementation of the mathematical models and algorithms described in the previous chapter. It provides a detailed description of how these models were translated into computer code and integrated into the optimization software. As concluded in section 3.3.1 the optimization models can be address having a MILP approach, increasing computational efficiency and reuducing problem complexity. The implementation details of the optimization software are also provided. This includes information on the programming language used, the software libraries or frameworks utilized.

Additionally, the chapter highlights any challenges or considerations encountered during the implementation process. It discusses issues related to data handling, algorithm scalability, convergence criteria, and computational resources. Overall, in this chapter the mathematical representation and analysis become practical and tangible to give a software tool that satisfies the main objective of the thesis; develop an instrument that support decision and policy makers on shaping energy transition by easily create and asses different energy scenarios from a single to a multiple site perspective.

4.1 Tool's Architecture

Figure 4.1 illustrates a general web application architecture that serves as a reference for developing the tool. The architecture encompasses various components, starting with the local data allocation in memory (database). Then, The backend consists of two main layers: the automated database management and the data interaction request within the PVGIS API composed the Data layer, the operational layer is where optimization and mathematical models are employed. The frontend comprises the presentation layer, which acts as a gateway for user requests and backend responses. This layer facilitates active interaction with data through dashboards, allowing users to actively engage with the application. Additionally, Figure 4.2 presents the block diagram of the application's functionality, providing a visual representation of the expected inputs and outputs. The diagram outlines the sequential steps involved in utilizing the tool and showcases the interaction between different components. Starting with the user input, which include the

location's name and its decimal latitude and longitude, alongside the hourly energy demand for a requested period (maximum 25 years).

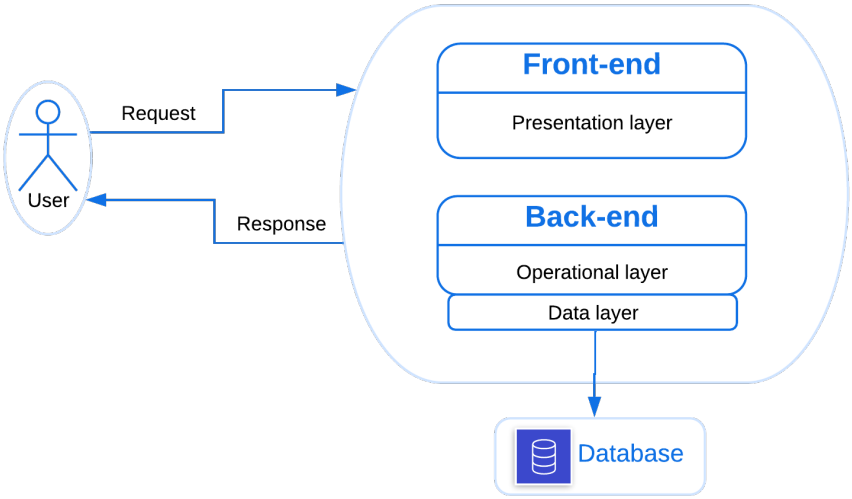

Figure 4.1: Standard web application architecture.

As the inputs are received, they are passed to the data request and optimization models within the operational layer. The required data is obtained through the utilization of the PVGIS API, which offers hourly data for variables such as global horizontal irradiance with optimal tilt angles ($G(t)[W/m^2]$), wind speed at 10 meters above sea level ($WS10m(t)[m/s]$), and air temperature ($T2m(t)[°C]$). It is important to note that the tool utilizes the SARAH-2 database, which encompasses satellite-based climate data for Europe, Asia, and Africa from the years 2005 to 2020 [28]. This extensive database serves as a valuable resource for accessing reliable and comprehensive climate information within the tool.

To proceed with energy scenario simulation, the user is required to provide additional input parameters related to financial and energy limits. These parameters include the discount rate, which determines the present value of future cash flows, and the limit on the maximum generation capacity, which represents the maximum allowable energy generation capacity for the system.

Once all the parameters are inputted, the simulation process begins. The mathematical and optimization models within the operational layer utilize these parameters, along with the previously mentioned inputs such as energy demand, renewable energy generation data, and system constraints. These models perform calculations and optimizations to simulate and analyze different energy scenarios. In tables 4.2 and 4.3 are listed the required inputs.

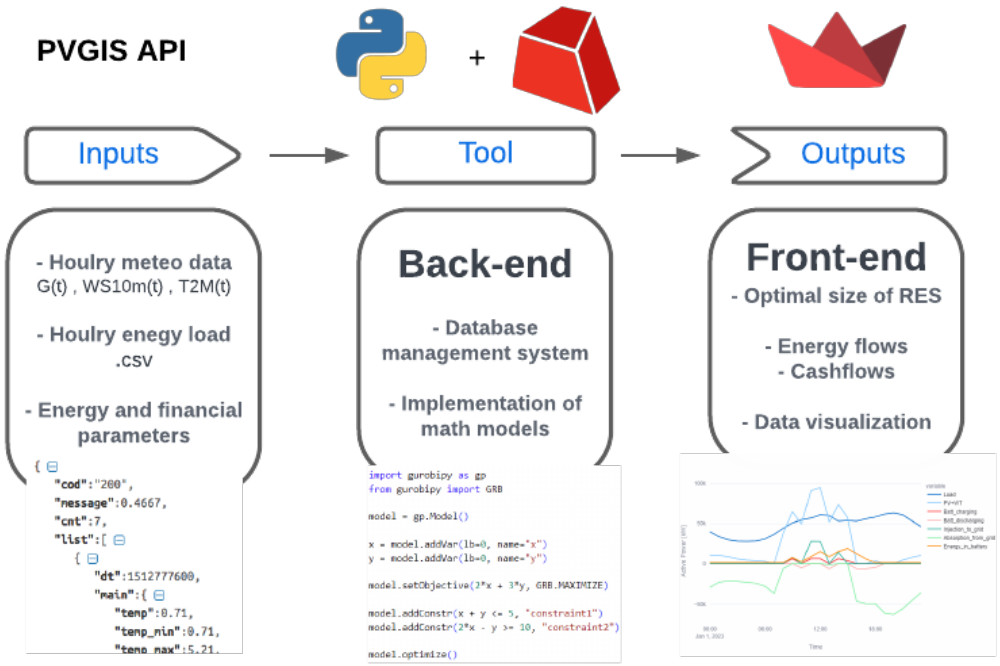

Figure 4.2: Tool's block diagram.

By incorporating the user-inputted parameters, the mathematical and optimization models play a crucial role in conducting the energy scenario simulations. They enable the exploration of various scenarios, allowing users to assess the financial and energy feasibility of different system configurations and make informed decisions based on the simulation results.

Lastly, the data visulaization is performed by the Python library *streamlit*, in this dataplotter the user can visualize the daily, monthly, and yearly energy and financial profiles; the summary table resulsts as well.

4.2 Implementation

In the implementation of mathematical models into a software system, a modular program approach involves breaking down the software into self-contained modules, each responsible for a specific mathematical model or component. By modularizing the program, it becomes more flexible and easier to modify individual modules

without affecting the entire system. Moreover, this approach enables the integration of various mathematical models seamlessly, allowing the software to handle complex calculations efficiently. Additionally, the use of standardized interfaces between modules ensures interoperability and simplifies the integration process.

Being Python an object-oriented programming language makes it appropriate to have a modular program approach. Figure 4.3 illustrates the modules inside the developed tool, in total there are three modules which are called from the *Main.py* function.

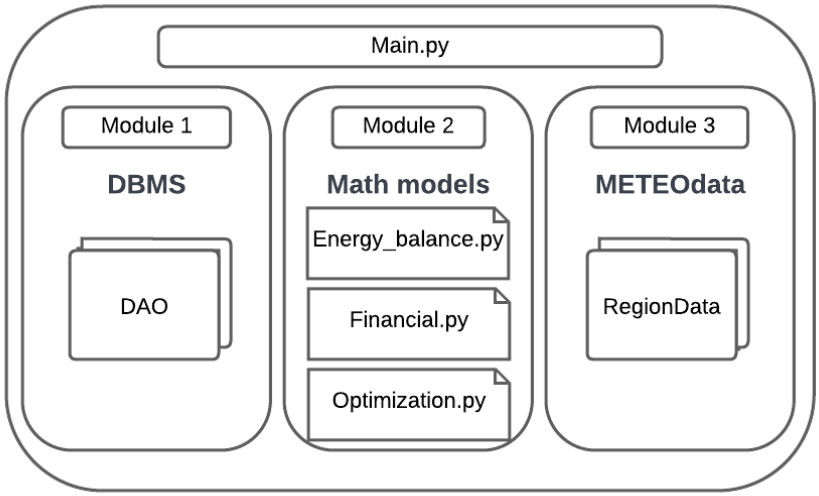

Figure 4.3: Tool's modular programming structure.

The first module oversees the administration of the database (DBMS) within the accounts by employing a data access object (DAO) class. This DAO class encompasses all the relevant attributes for facilitating communication with the local database, enabling the execution of various queries and the flexibility to get acces to database from any script in the program. To fulfill the program's requirement for analyzing multiple regions, the third module incorporates the RegionData class to facilitate communication with the PVGIS API. This integration enables the program to make multiple requests for meteorological data while it is running, facilitating efficient data retrieval for various regions. Lastly, The second module is where the energy, financial and optimization functions are implemented. Module 2 represents the logic and analysis explained in section 3.

The tool's development has been facilitated by various Python libraries, as detailed in Table 4.1. Pandas has been instrumental in the overall design, being

widely used across all modules to efficiently manage and structure data. Gurobipy has played a crucial role by providing the interface necessary for implementing optimization models. Furthermore, Streamlit has proven invaluable in creating a user-friendly interface and enabling users to interact with the tool through different inputs commands.

Table 4.1: Python libraries used inside each module

Module 1	Module 2	Module 3	Main
Sqlalchemy	Pandas	json	Streamlit
Pandas	SciPy	Requests	Folium
Mysql	NumPy	Pandas	Geopandas
Datetime	GurobiPy	io	Plotly

The libraries used in each module have significantly contributed to the development of the program as a whole. Here is a more detailed description of each library and its role in enhancing the functionality of the respective modules:

- Pandas: widely used for data manipulation and analysis. It provides data structures and functions to handle structured data, making it easier to work with database queries and data extraction [35].
- Sqlalchemy: provides a high-level interface for interacting with databases using SQL. It allows for the creation of database connections, execution of queries, and handling of database transactions [36].
- NumPy: provides support for numerical computations in Python. It is often used for handling numerical data and performing calculations on database results [37].
- SciPy: builds on top of NumPy and provides additional functionality for scientific computing. It includes modules for optimization, interpolation, integration, signal processing, and more. It can be useful for implementing complex mathematical models and algorithms [38]
- Requests: is commonly used for making HTTP requests in Python. It allows for sending requests to the PVGIS API and retrieving the corresponding meteorological data.
- json: provides functions for working with JSON data. It can be used to parse the API responses, extract the required data, and convert it into a usable format.

- Gurobi: Gurobi is a commercial optimization solver that can be used to solve mathematical optimization problems. It provides a high-level interface for formulating and solving linear programming, integer programming, and quadratic programming problems [39].

- Streamlit: library for building interactive web applications for data science and machine learning. It provides a simple and intuitive interface for creating interactive dashboards, visualizations, and data exploration tools [40].

- Plotly: library for creating interactive and customizable plots and visualizations. It supports a wide range of chart types, including line plots, scatter plots, bar plots, pie charts, and more. Plotly provides an API that allows you to create interactive plots with features like zooming, panning, and hover tooltips [41].

The code of each module is shown and commented in annexes. However, in the following will be shown a pseudo-code representation of the code implementation, regarding the energy production from RES and Gurobi optimization model.

Listing 4.1: RES generation model implementation (Pseudo-code)

```
# Import libraries
import pandas as pd
from functions_constants import constants as c_eb
import scipy.interpolate

def RES_generation(df):
    # PV production model
    df['G(i)'] = df['G(i)']/1000 #irradiance in kW
    df['PV_cell_temperature'] = equation 3.4
    df['PV_eta_thermal'] = equation 3.3
    df.loc[df['G(i)'] > c_eb.PV_G_0, 'PV_DC'] = equation 3.1
    df.loc[df['G(i)'] > c_eb.PV_G_0, 'PV_production'] = equation 3.5

    # Wind Turbine (WT) production model
    df['U_w'] = equation 3.6
    scipy.interpolate.interp1d(wind_speed, power_turbine)
    df['WT_production'] = equation 3.7

    # simulate ageing of plant production
    ageing_factor = 0,5%
    for year in range(year + 1, end_year):
        PV_production *= (1 - ageing * year)
        WT_production *= (1 - ageing * year)

    return df
```

As it can be noticed the code implementation makes reference to the equations explained in section 3, The imported script "constants" makes reference to the assumed constants for PV and WT technologies, which in Tables 4.2 and 4.3 are the listed values and their description. The code conducts simulations to estimate the aging of the power plants for each year, after the initial year. The aging factor applied is 0,5%. After completing the simulations, the code returns a dataframe containing the hourly local generation from RES.

Table 4.2: PV technology parameter values

Parameter	Value	Description
η_{dirt}	97%	Losses due to dirt
$\eta_{reflect}$	97%	Losses due to reflection
$\eta_{mismatch}$	97%	Losses due to mismatch
η_{cable}	99%	Losses in cable
γ	-0.005 [$°C^{-1}$]	Power reduction coefficient
G_0	0.017 [kW/m^2]	Minimum radiation coefficient
G_{STC}	1 [kW/m^2]	Radiation in STC
T_{STC}	25 [$°C$]	PV cell temperature in STC
$NOCT$	45 [$°C$]	Normal operating cell temperature
P_{nom}^{PV}	1 [MW]	Nominal power of a PV cell

Table 4.3: WT technology parameter values

Parameter	Value	Description
H_{hub}	93 [m]	WT hub height
H_{ref}	10 [m]	Height reference
z_0	0.1 [m]	Reference terrain roughness
P_{nom}^{WT}	2 [MW]	Nominal power of a WT

The flexibility of the simulation parameters is a notable aspect to highlight. Although the user has the ability to modify these parameters directly in the code, the values presented here were specifically chosen for the purposes of this thesis. The Gamesa 2MW wind turbine was selected for the simulations, and its power curve is depicted in Figure.

The implementation of the optimization model in the code follows the same structure as the mathematical model. The pseudo-code in Listing 4.2 outlines the steps for constructing an optimization model using Gurobi. The model defines decision variables, constraints, and an objective function. The solver then finds the solution that satisfies the model, typically within seconds or a few minutes, depending on the size of the dataframe and on the feasibility region of the model.

The initial stage involves taking the dataframe obtained from the RES_generation function, which comprises data on PV and WT power generation along with hourly energy load. Using this data as a basis, decision variables are established with suitable constraints, limiting them to positive, negative, or both values. By employing a solver, the optimal values for the quantity of PV panels (n_pv), wind turbines (n_wt), and storage capacity (c_s) are determined, aiming to maximize self-sufficiency and minimize dependence on the grid.

The second input of the function $optimal_model$ (opt_data) stands for the inputted simulation parameters by the user which will be better explained in the following subsection.

Listing 4.2: Optimization model implementation (Pseudo-code)

```
# Import libraries
import gurobipy as gp
from gurobipy import GRB

def optimal_model(df,opt_data):

    # Create the model
    m = gp.Model("Max_SS_Min_Absorption")

    # Define decision variables
    # Undependent of time
    n_pv = m.addVar(positive, type = continuous) # number of PV
    n_WT = m.addVar(positive, type = continuous) # number of WT
    c_s = m.addVar(positive, type = continuous) # Storage capacity

    # Dependent of time
    Eb(t) = [m.addVar(positive, type = continuous) {length(df)}]
    Pb(t) = [m.addVar(+/-, type = continuous) {length(df)}]
    P_inj(t) = [m.addVar(positive, type = continuous) {length(df)}]
    P_abs(t) = [m.addVar(negative, type = continuous) {length(df)}]
    PG(t) = equation 3.25 {length(df)}

    # Financial expressions
    NPV(t) = equation 3.21

    # Define constraints
    # Power Balance:
    m.addConstrs(PG[t] - Pd[t] - Pb[t] - P_inj[t] - P_abs[t] = 0)

    #Financial:
    m.addConstr(NPV >= 0)

    # Battery:
```

```
m.addConstr(Eb[t = 0] = 0.2 c_s)
m.addConstr(Pb[t = 0] = 0)
m.addConstrs((Eb_t[t] >= 0.2 * c_s )
m.addConstrs(Pb[t] >= -c_s)
m.addConstrs(Pb[t] <= c_s)
m.addConstrs(Eb[t] = Eb[t-1] + Pb[t])
m.addConstrs(Big M method constraints)

# Set objective
m.setObjective(gp.quicksum(P_abs), sense=gp.GRB.MAXIMIZE)

# Optimize the model
m.optimize()
```

As mentioned in section 3.3.1 one of the main concerns for the implementation was the computational cost the optimization model could have. Even though the model is totally linear, the fact of dealing with large datasets of decision variables and constraints affect the convergence inside a feasible region. Therefore, an arrangement for the solver settings had to be adopted. According to Gurobi documentation [39], it is possible to set parameters to constraint the convergence inside a feasible solution. The configuration of parameters used for the model refers to mix-integer programming (MIP) strategies, in listing 4.3 are shown the ones use for solve the single-site model. "$MIPGapAbs$" refers to the gap tolerance between the objective value and the best bound value, in this case has been set as less or equal to 10%. "$MIPFocus$" is established to indicate the solver how to prioritize exploration, a value of 1 instruct to perform the search space evenly. "$Method$" the parameter specifies the algorithmic approach used by the solver, the value of 2 suggests to the solver to prioritize good feasible solutions over rigorous optimal ones. Lastly "$Corssover$" indicates whether or not the crossover method is implemented inside the model, in this case has been set to 0 in order to do not use it, because enable it means higher computational cost for the solver.

Listing 4.3: Parameters for mix integer programming

```
m.setParam("MIPGapAbs",0.1) # Maximum tolerance for convergence
m.setParam('MIPFocus', 1) # Indicates how the solver explores
m.setParam('Method', 2) # Algorithmic approach selection
m.setParam('Crossover', 0) # Crossover method
```

It is worth noting that the generation and storage capacities remain constant and independent of time. This implies that the energy system installation is considered to occur at the start of the analysis period, and it is assumed that there will be no increase in capacities over time. This fact also influences on the computational cost and faster convergence. The results for convergence time will be presented

inside the case study chapter.

Despite initially having a well-described optimization model, the implementation process encountered various challenges. To address these complications, multiple simulations and trials were conducted in order to reach the current state where the model can effectively utilize the solver to find an optimal solution. By fine-tuning these parameters and making appropriate adjustments discussed in this section, the model has been refined to a point where it can efficiently utilize the solver and offer improved performance in finding an optimal solution.

4.3 Build a Single-site energy scenario

After running the command line "*streamlit run Main.py*" on the system's terminal, the program will be opened in a web page with four different tabs. From the main page the user will be able to add or delete site's hourly METEO data to/from the local database. As depicted in Figure 4.4 the required inputs are Province name, Site name, latitude, longitude and the period in years of the data the user wants to add. The modules used in this Tab are the module one and three which allows the connection with PVGIS API and then allocate the downloaded data in the local database.

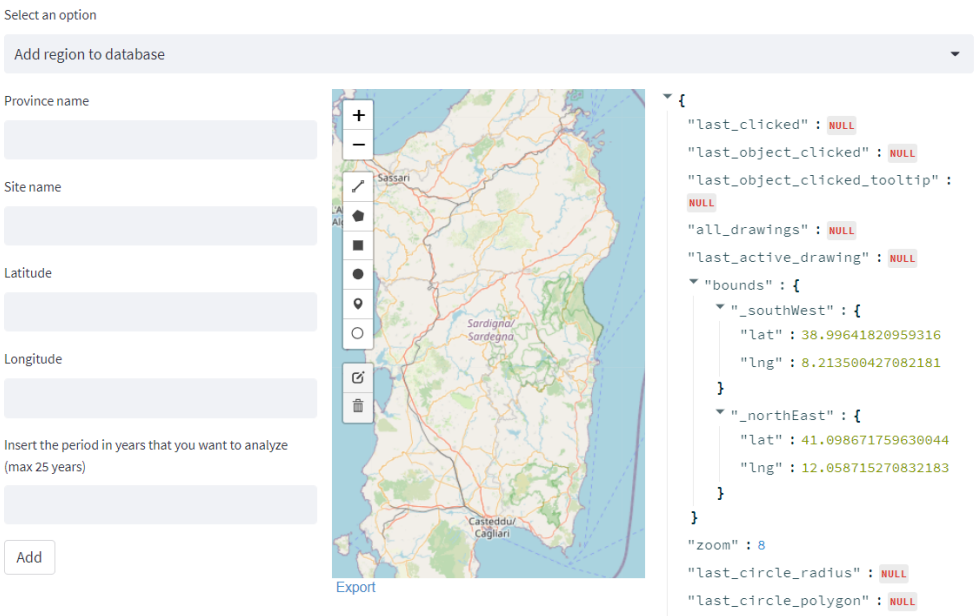

Figure 4.4: Tab 1. Add/delete region to/from database

To facilitate the single-site scenario simulation, the user is provided with an interactive table that displays the available regions within the database. This table includes the coordinates of each region and the length of the hourly data, which spans from the minimum date (Min_date) to the maximum date (Max_date). The data in this table can be easily edited to input desired values.

	Province	Region	Latitude	Longitude	Min_date	Max_date
	OT	olbia_1	41.1	9.3	2030-01-01 00:00:00	2054-12-31 23:00:00
	CA	cagliari_1	39.232	9.119	2030-01-01 00:00:00	2054-12-31 23:00:00
	OR	oristano_1	39.89	8.593	2030-01-01 00:00:00	2054-12-31 23:00:00
	NU	nuoro_1	40.464	9.459	2030-01-01 00:00:00	2054-12-31 23:00:00
	OG	ogliastra_1	39.866	9.55	2030-01-01 00:00:00	2054-12-31 23:00:00
	VS	medio_1	39.597	8.663	2030-01-01 00:00:00	2054-12-31 23:00:00
	SS	sassari_1	4.758	8.703	2030-01-01 00:00:00	2054-12-31 23:00:00
	CI	carbonia_1	39.244	8.562	2030-01-01 00:00:00	2054-12-31 23:00:00

Name this case scenario:

Simulate

Figure 4.5: Tab 2. Single site simulation

In addition to the region information, the simulation requires several parameters related to financial aspects, generation limitations, and grid constraints. These parameters are presented in Table 5.5 along with their corresponding descriptions and units. These values can be adjusted according to the specific requirements of the simulation. Finally, the user can name a new energy scenario in order to simulate the sites desired. In this sense, Gurobi solver will manage each optimization model for the regarding regions, the outcome will be their respective optimal values for generation and storage capacities for each energy system modelled. Furthermore, the solver is capable of reconstruct the hourly profiles for each decision variable that must be compliant with constraints and results. At the very end the program will return a reconstructed and detailed dataframe for each site and allocate it inside the database with the name of the case scenario, the data can then be used

for data visualization and analysis, see section 4.4.

As previously described, the integration of the front-end and back-end components provides flexibility in creating various energy scenarios. This flexibility enables the simulation of different regions as well as the simulation of the same region with different input parameters. Users can compare results across different time periods, financial parameters, and technology specifications within the modeled energy system. This capability allows for comprehensive analysis and comparison of diverse scenarios.

Based on the inputs provided, the solver's outcome from the single-site model can be valuable for decision-makers, as it will determine whether the model is feasible or infeasible. If the model is feasible, it means that there exists a set of decision variables that satisfies all the defined constraints, and an optimal solution has been found. In this case, decision-makers can use the results to make informed decisions regarding the installation of the energy system at the specific site.

On the other hand, if the model is infeasible, it indicates that there are no feasible solutions that meet all the constraints. In this situation, decision-makers may need to reassess their inputs, constraints, or objectives to find a feasible solution. Identifying infeasibility can be crucial for decision-making, as it may signal the need for adjustments or revisions in the planning and design of the energy system.

Table 4.4: Input parameters for single-site simulation

Parameter	Units	Description
MaxC_PV	MW	Maximum installable capacity of PV
MaxC_WT	MW	Maximum installable capacity of WT
Max_Injection	MW	Maximum injection to grid
IRR	%	Internal rate of return
Ele_price	€/kWh	Cost of energy purchase
Sell_price	€/kWh	Energy selling price
uCostPV	€/kW	Unit cost of PV installation
uCostWT	€/kW	Unit cost of WT installation
uCostStorage	€/kW	Unit cost of storage installation
Discharge_time	h (1-24)	Battery discharge time
mCostPV	€/kW	Maintenance cost of PV
mCostWT	€/kW	Maintenance cost of WT
eNPV	€	NPV value at the end of simulation

4.4 Build a Multiple-site energy scenario

The multiple-site energy scenario can be built by adding the energy network constraints that interconnect all the possible evaluated regions inside the model. The user is asked to provide the grid topology and its characterization by constructing the PTDF explained in section 3.3.2.

In order to perform the implementation inside the code the line reactance plays an important roll determining the line limits. As mentioned the voltage levels considered inside the model correspond to 220 kV and 380 kV, then their respective reactance need to be calculated in order to properly implement the PTDF calculation inside the model, the reactance are expressed as:

$$X_{i,j}^{220kV} = 0.67\Omega/km \quad \rightarrow \quad \tilde{X}_{i,j}^{220kV} = \frac{X_{i,j}^{220kV}}{Z_{base}^{220kV}}$$
$$X_{i,j}^{380kV} = 0.23\Omega/km \quad \rightarrow \quad \tilde{X}_{i,j}^{380kV} = \frac{X_{i,j}^{380kV}}{Z_{base}^{380kV}}$$

Where $\widetilde{X}_{i,j}$ represents the normalized (p.u) value of the reactance and:

$$Z_{base}^{220kV} = \frac{(220kV)^2}{100} \qquad Z_{base}^{380kV} = \frac{(380kV)^2}{100}$$

In this case the subscripts i and j represent the $from-bus$ and $to-bus$ respectively. In this sense it is expected the list for both type of buses inside the network, the connection between two busses result in a branch with length $'l'$ (km). Afterwards, the connection matrix can be built which represents for each row the branches and for each column the buses. The connection matrix C_{ft} can be implemented inside the code as an $sparse$[1] matrix where per convention the indices 1 represent the $from-buses$ and -1 the $to-buses$, it can be formulated as follows:

[1]Sparse matrix is a matrix that contains mostly zero elements. By exploiting the sparsity of the matrix, computational efficiency and memory savings can be achieved.

$$C_{ft} = \begin{bmatrix} 1 & 0 & 0 & \dots & 0 & -1 & 0 & \dots & 0 \\ 0 & 1 & 0 & \dots & 0 & 0 & -1 & \dots & 0 \\ \vdots & \vdots & \vdots & \ddots & \vdots & \vdots & \vdots & \ddots & \vdots \\ 0 & 0 & 0 & \dots & 1 & 0 & 0 & \dots & -1 \end{bmatrix}_{nl \times nb}$$

Where nl is the vector length for branches or lines, and nb represents the vector length for buses.

The PTDF can be calculated after representing the reactance in terms of susceptance, which is the reciprocal of reactance $Bf_{i,j} = \tilde{X}_{i,j}^{-1}$. The suscenptance matrix can be constructed as represented in the following cases being; b_i is the series susceptance associated to the i^{th} branch, the positive values of b_i placed for the $from - buses$ and the $-b_i$ for the $to - buses$, otherwise is 0. Therefore, the power injection at each $from - bus$ can be denoted as the B_{bus} matrix express it as in equation 4.1.

$$Bf_{ij} = \begin{cases} b_i & \text{if } j = f_i \text{ (from bus of branch } i) \\ -b_i & \text{if } j = t_i \text{ (to bus of branch } i) \\ 0 & \text{otherwise} \end{cases}$$

$$Bf = \begin{bmatrix} b_1 & 0 & 0 & \dots & 0 & -b_1 & 0 & \dots & 0 \\ 0 & b_2 & 0 & \dots & 0 & 0 & -b_2 & \dots & 0 \\ \vdots & \vdots & \vdots & \ddots & \vdots & \vdots & \vdots & \ddots & \vdots \\ 0 & 0 & 0 & \dots & b_{nl} & 0 & 0 & \dots & -b_{nl} \end{bmatrix}_{nl \times nb}$$

$$Bbus = {C_{ft}}^T \cdot Bf \tag{4.1}$$

The calculation of the PTDF values involves multiplying the i^th row of the Bf matrix with the k^th column of the inverse Bbus matrix, yielding a scalar value. This mathematical expression represents the calculation of the PTDF values, indicating the sensitivity of branch DC power flows to changes at the non-slack buses. The PTDF matrix is constructed according to the following cases:

$$\text{PTDF}_{ij} = \begin{cases} Bf_{ik} \cdot Bbus_{kj}^{-1} & \text{if } j \in \text{noslack} \\ 0 & \text{otherwise} \end{cases}$$

Once the PTDF for the network under analysis is constructed, the user can start modelling the energy scenario. As a starting point, the program will suggest

to which transmission line each region's energy system should be connected, it will predominate the closest line for the region i^th. This features will allow the program to calculate the respective reactance according to the connection, this will allow to set the boundaries for power injection. In this thesis, it is assumed maximum values for power injection at 220 kV and 380 kV transmission lines 200 MW and 1100 MW respectively.

In Figure 4.6 is represented a general grid composed by 220 kV and 380 kV transmission lines and the regions that are composing the model. What is yet to be represented in the figure are the virtual generators that constitute the model for HVDC lines that are connected to mainland. In this sense, the virtual generators have bi-directional flows simulating the absortion or injection behavior of HVDC transmission lines.

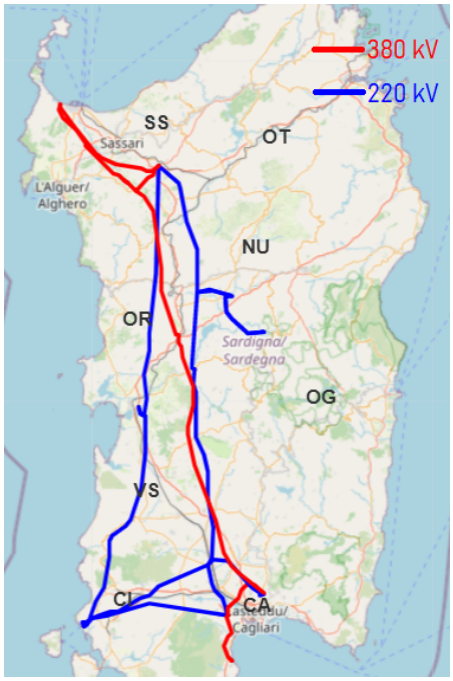

Figure 4.6: Provinces location and Medium/high voltage electricity grid in Sardinia.

In Figure 4.6 the acronyms for the regions shown stand for Cagliari (CA), Sassari (SS), Olbia Tempio (OT), Nuoro (NU), Oristano (OR), Medio Campidano (VS), Carbonia Iglesias (CI) and Ogliastra (OG). In chapter 5 will be also used.

At this point the model is about to be simulated, what is still missing is to provide the limits for the virtual generators, in order to set the boundaries for the

power absorption and injection from/to mainland.

$$P_v^{min} \leq P_{abs,v}^{mainland}(t) \leq P_v^{max}$$
$$P_v^{min} \leq P_{inj,v}^{mainland}(t) \leq P_v^{max}$$

The outcome from the simulation will give the values of optimal generation and storage capacities for each region i that satisfies the constraints, specially for multiple-site having under consideration the interconnections between regions through the electrical netwrok. In this sense, the results will be compliant for the maximum optimal values of SS, thus the minimization of reliance from grid mainland.

4.5 Results Visualization

Tab number four of the application is dedicated to data visualization. Once the simulation is completed, the program saves and stores the results in the database inside a table called as the case scenario. To facilitate analysis and provide users with a wide range of possibilities to evaluate each scenario, a graphical interface with interactive plots has been developed.

The interactive nature of the plots allows users to visualize and analyze the results at various levels of detail, ranging from hourly to yearly basis. This flexibility enables users to explore the data in different time frames and easily identify patterns or trends. For instance, they can identify periods when power generation is higher or when the absorption from the grid becomes more critical. As shown in Figure 4.7, the graph on the left-hand side provides users with the option to select hourly profiles from a range of dates. This graph allows users to visualize the data at a granular level, examining the variations in values throughout specific time periods.

On the other hand, the graph on the right-hand side presents a bar version of the hourly profiles. However, instead of displaying individual values, it shows the cumulative values for all the years that have been simulated. This cumulative representation provides an overview of the aggregated data over time, highlighting the overall trends and patterns.

The identifier "*cagliari_1*" represents the results for the specific region being evaluated. In the application's dropdown lists, users can easily switch between different regions that were simulated within the case study. This allows for a convenient way to compare and analyze results across various regions. Additionally,

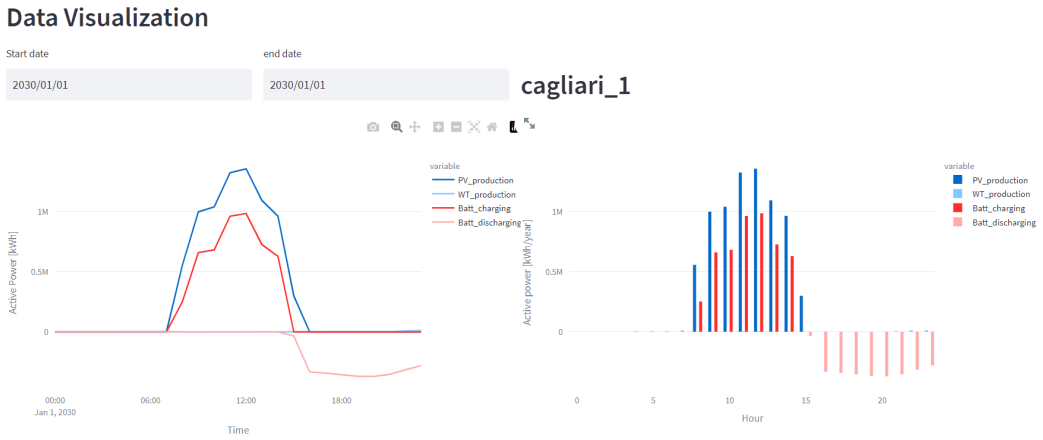

Figure 4.7: Tab 3. Results visualization

another dropdown list is available to select the specific magnitudes or variables that users wish to analyze. In Figure 4.7, the depicted variables are the production from PV panels, wind turbines, and the behavior of the battery in terms of charging and discharging. By providing these dropdown lists, the application enables users to explore and analyze the simulated data for different regions and variables of interest. This flexibility empowers users to gain insights into the performance and behavior of renewable energy generation, storage systems, and other relevant parameters specific to each region. Furthermore, the graphical interface offers additional features such as the ability to customize the appearance of the plots, add annotations or markers, and compare different scenarios side by side.

Figure 4.8 displays additional graphs within the data visualization section. One of the graphs represents a box plot showing the distribution of the magnitude being investigated. This box plot provides insights into the variability and range of the data, allowing users to understand the statistical characteristics of the variable under consideration. Another graph focuses on the economic aspects of the energy system. It presents the cumulative Net Present Value (NPV) profiles for the entire evaluation period. This visualization offers a comprehensive view of the financial performance of the energy system over time, providing valuable information on the economic viability and profitability.

Furthermore, the figure includes a summary section that highlights the most important parameters for each individual site. This summary includes key information such as the SS and SC values, the number of PV panels, the number of WT, the storage capacity, and other relevant parameters. This summary enables users to quickly assess and compare the results for each site, facilitating the identification

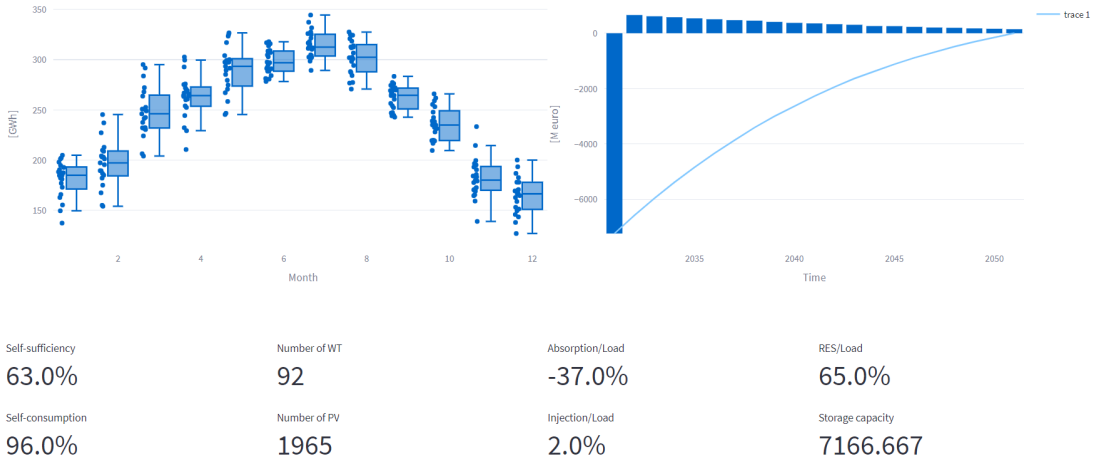

Figure 4.8: Tab 3. Economic results

of the most significant factors and their impact on the overall system performance.

By incorporating these additional graphs and the summary section, the application provides a comprehensive and easily accessible overview of the results. Users can gain insights into the statistical characteristics, economic performance, and key parameters for each site, supporting informed decision-making and detailed analysis of the simulated scenarios.

To evaluate the capabilities of the tool, a specific case study has been chosen for testing purposes. The case study introduced in chapter 5 represents a specific scenario or system that will be simulated and analyzed using the tool's functionalities. The selection of a case study allows users to apply the tool to a real-world scenario or problem of interest. It serves as a practical example to assess the tool's effectiveness in addressing specific challenges or objectives related to energy systems, renewable energy integration, or other relevant domains.

Chapter 5

Case Study: The Green Electrification of Sardinia

The Sardinia project is a pilot that could be exported nationwide and calibrated to suit local differences and requirements. Sardinia could thus become Europe's greenest island and a model for Italy as a whole. As reported in [42] the island is conceiving big attention by Europe as it is a perfect example of Distributed Energy Resource (DER), Sardinia brims with the potential to become a large-scale laboratory for electrification and sustainability. The project has a bold vision to bring about a significant transformation in Sardinia's energy model by 2030, aiming to deliver environmental, social, and economic benefits to the entire region and its community.

Its main objective is to drive a radical shift away from fossil fuel-based energy production and instead increase the proportion of energy generated from solar and wind power sources. Currently, only 7% of energy in Sardinia comes from photovoltaic systems, while wind power accounts for 15% [4]. Therefore, the project seeks to substantially boost these percentages and promote renewable energy as a cleaner and more sustainable alternative.

Looking ahead, Sardinia envisions a future characterized by further advancements in its energy system. The upcoming years hold promising prospects for the island, driven by key projects and initiatives. One notable development is the Tyrrhenian Link, which aims to connect Sardinia's electricity grid with the mainland, facilitating greater access to renewable energy sources and ensuring a more reliable and sustainable energy supply. Additionally, Sardinia is committed to embracing the

concept of green electrification, encompassing the integration of renewable energy generation, energy storage systems, and smart grid technologies. This holistic approach seeks to optimize energy efficiency, reduce emissions, and promote a more sustainable and resilient energy system across the island [43].

For the purpose of this study, the University of Cagliari has provided valuable data on hourly energy consumption and purchase/selling electricity prices in Sardinia for the years 2030 and 2050 for each province. This data serves as a crucial foundation for analyzing and evaluating the energy landscape in the region during these time-frames. This chapter provides a comprehensive overview of Sardinia's current energy system, laying the groundwork for modeling and analyzing different future energy scenarios from a province to island level, using the tool reported in section 4.

By combining projected data and advanced optimization techniques, the chapter aims to provide simulation results and valuable insights about the tool's performance, tested with a real case scenario with a reliable projected energy demand and financial inputs. The outcome can assist decision-makers and policy-makers in shaping the energy landscape of Sardinia.

5.1 Current Sardinia's energy scenario

At present, Sardinia's energy generation largely depends on traditional power plants, including those fueled by coal. This heavy reliance on fossil fuels poses significant challenges in terms of greenhouse gas emissions and contributes to the overall carbon footprint of the island, as represented in Figure 5.2 the carbon intensity per electricity consumed in 2023 round the 600 gCO_{2eq}/kWh. According to Terna the potential disconnection of Sardinian consumers from the electrical network becomes a significant concern when there is no generation from coal power plants [44].

The Figure 5.1 illustrates the active fossil fuel power plants in Sardinia. According to the plans, Fiumesanto and Sulcis are expected to cease their operations by 2025. As a result, Sardinia aims to become carbon-free by 2030, indicating that Sarlux power plant will also be decommissioned [44]. Since this study focuses on the period between years 2030 and 2050, one of the energy scenarios will solely consider Sarlux as the remaining power plant in operation.

Despite the high reliance Sardinia has on coal power plants, the period from 2010 to 2020 witnessed a notable expansion in the share of renewables, as depicted

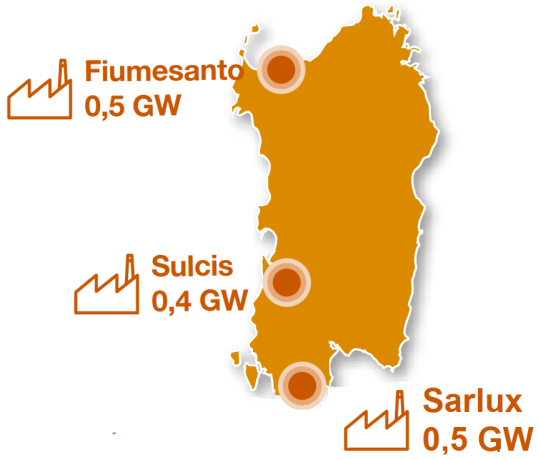

Figure 5.1: Sardinia's active Fossil fuel power plants. Adapted from [44]

in Figure 5.3. This increase is primarily attributed to the growing contribution of photovoltaic (PV) and wind energy systems, reflecting a significant rise in the energy generated from these sources inside the island.

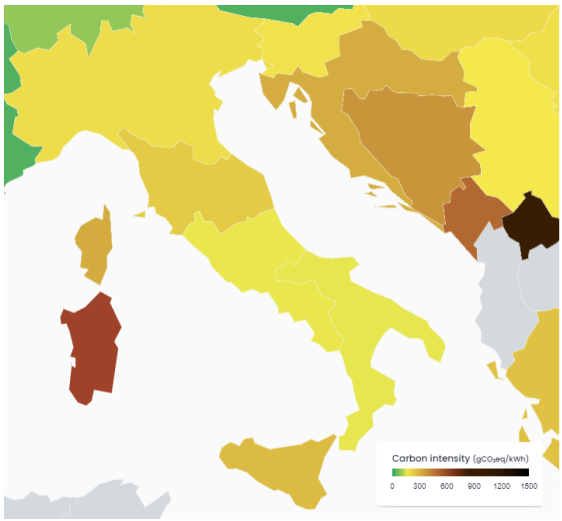

Figure 5.2: Carbon intensity per electricity consumed (gCO_{2eq}/kWh) in Italy. Taken from Electricity Maps [45] on May 2023

One notable achievement in Sardinia's energy transition is the projected reduction in coal power plants. Recognizing the harmful environmental impacts associated with coal plants, Sardinia has made significant progress in phasing out these facilities. Instead, the focus has shifted towards increasing the proportion

of energy derived from renewable sources. The adoption of renewable energy technologies, such as solar and wind power, has gained momentum, enabling the island to harness its abundant natural resources and reduce its dependence on non-renewable energy. Achieving values up to 2 TWh and 1.2 TWh for Wind and PV technologies respectively in 2020, according to Figure 5.3.

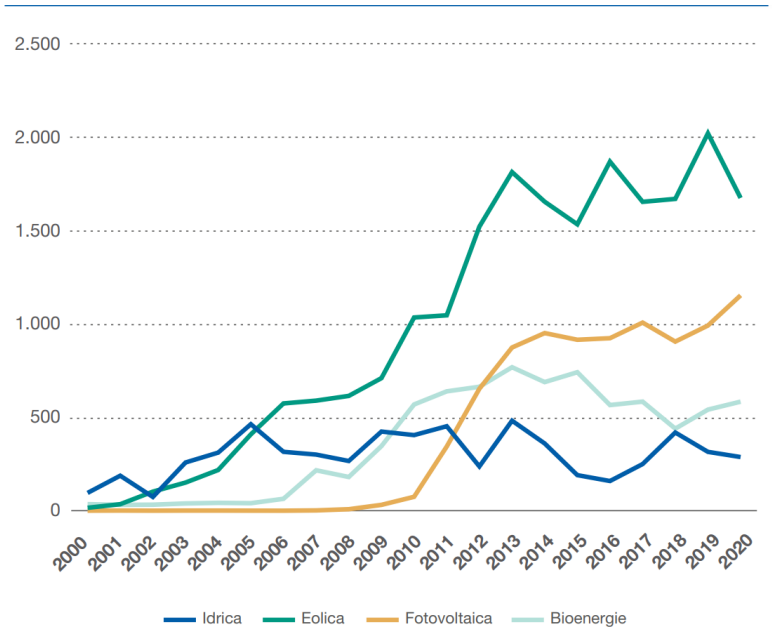

Figure 5.3: Increase share of renewable energy generation in Sardinia (GWh) [46]

With respect to the current situation of Sardinia's electrical grid and the existing High Voltage Direct Current (HVDC) links with mainland, the island relies on two main connection cables: Sacoi, which links the island with Corsica, and Sapei, which provides the crucial connection to the mainland peninsula as illustrated in Figure 5.4. However, the existing transmission lines face limitations in terms of capacity and reliability, posing challenges to the integration of renewable energy sources and ensuring a stable electricity supply.

To facilitate the growth of renewable energy generation in the region, it is crucial to ensure that the existing electricity transmission infrastructure can support the increased capacity. Terna, the transmission grid operator, has recognized this need and has initiated several network expansion projects. Inside the Development Plan of 2021, The Tyrrhenian link is positioned as one of the most important inside it, which main objective is to stabilize and secure the power grid, ensuring efficient exchange between the two islands, Sardinia and Sicily, and the mainland [43]. Figure 5.5 represents the connections of the Tyrrhenian link.

Figure 5.4: Current transmission lines connected to mainland. Adapted form Entsoe grid map [47]

5.2 Preliminary analysis

The analysis begins by assessing the energy demand projections for the eight provinces in Sardinia. According to a forecast conducted by Cagliari University for 2030, the total energy consumption of the entire island is estimated to reach 9.7 TWh. However, it is anticipated that a portion of this demand will already be met by existing hydroelectric and thermal plants, such as Sarlux in Cagliari, which might be programmed for phase out by 2030. As a result, the remaining energy demand is intended to be fulfilled by non-conventional generation methods, particularly through the use of photovoltaics, wind farms, and electrochemical storage.

Table 5.1 presents the projected energy production by conventional generators for each province in 2030, being the hydrolectric in Nuoro with the higher contribution, up to 295.783 GWh/year. On the other hand, Table 5.2 illustrates the energy demand per province that needs to be supplied by renewable generators. This

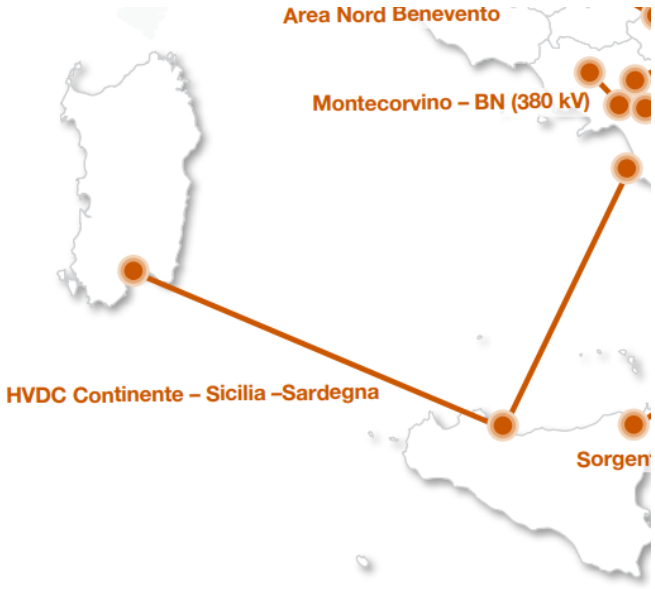

Figure 5.5: Tyrrhenian link, adapted from [44]

Table 5.1: Hydroelectric and thermal plants production in Sardinia by province in 2030 and 2050

Province	Hydroelectric (GWh)	Thermal plant (GWh)
CA	-	2.861
CI	-	-
VS	32.770	-
OR	22.600	-
NU	295.783	-
OG	45.200	-
OT	-	-
SS	10.498	-

calculation takes into account the subtracted production from hydroelectric and coal plants from the total energy demand for each province.

A noteworthy observation is that the provinces of Cagliari (CA), Carbonia-Iglesias (CI), and Sassari (SS) exhibit higher energy demands, collectively accounting for approximately 70% of the total energy consumption in the island for years 2030 and 2050 as represented in tables 5.2 and 5.3. This emphasizes the significance of these provinces in shaping Sardinia's overall energy landscape. To delve further into the energy dynamics of the region, the analysis focuses specifically on Cagliari province. At least two energy scenarios will be simulated for Cagliari, providing

a comprehensive outlook on potential future pathways. One scenario considers the continued generation from the Sarlux power plant, while another scenario explores the possibility of shutting down Sarlux and completely rely on alternative energy sources. The purpose of simulating these scenarios is to evaluate the island's potential to decrease its dependency on power plants fueled by fossil fuels, while simultaneously ensuring a significant degree of self-sufficiency and cost-effectiveness.

Table 5.2: Sardinia energy demand by province for the year 2030

Province	Energy demand (GWh)	Proportion
CA	3'048.44	0.32679
CI	1'868.34	0.20028
VS	403.19	0.04322
OR	1'054.91	0.11309
NU	664.26	0.07121
OG	183.84	0.01971
OT	408.94	0.04384
SS	1'696.55	0.18187
Sardinia	9'328.47	1

Table 5.3: Sardinia energy demand by province for the year 2050

Province	Energy demand (GWh)	Proportion
CA	3'935.437	0.3221
CI	2'241.601	0.1835
VS	526.415	0.0431
OR	1'345.974	0.1102
NU	920.170	0.0753
OG	256.250	0.0210
OT	745.254	0.0610
SS	2'247.812	0.1840
Sardinia	12'218.913	1

In the simulation, a constant increment was assumed for the energy demand between the years 2030 and 2050. This means that the energy demand was projected to increase steadily over this 21-year period. Provides a comprehensive timeframe for analyzing the dynamics of the energy system and identifying trends, patterns, and potential challenges that may arise as the energy demand increases over time. It allows decision-makers to assess the sustainability and resilience of the system and make informed decisions based on the projected energy demand trajectory.

Subsequently, the estimation of the maximum potential capacity for each generation and storage technology is a crucial step to facilitate the accurate simulation of energy scenarios. In [48], a comprehensive analysis is presented considering factors such as land availability and resource accessibility for Sardinia. This analysis provides estimations of capacities for various generation technologies, including Wind farms (onshore), PV farms, and PV rooftop installations, specific to each province. These estimations serve as a baseline for modeling the energy systems of the eight provinces under investigation.

The outcome potential capacities from the study are reported in Table 5.4 indicating the maximum achievable values, the optimization process ensures that the selected capacities align with economic and power balance limitations. On the other hand, when sizing the storage system, the analysis assumes no limitations on land availability. The maximum capacity of the storage system relies on satisfying power balance and economic constraints since it ensures the uninterruptible energy supply and represents the most expensive cost of replacement/maintenance of the entire energy system.

Table 5.4: Maximum capacity potential assumed for Sardinia and different provinces [48].

Province	**Max Potential Capacities (GW)**		
	PV	**Wind (onshore)**	**Storage**
CA	2.413	2.658	-
CI	6.514	7.514	-
VS	6.514	7.514	-
OR	7.112	7.835	-
NU	12.558	13.835	-
OG	7.113	7.864	-
OT	10.220	10.865	-
SS	19.243	21.199	-

5.3 Province level simulations and results

As explained in section 4.3 the first step is to provide the inputs in order to proceed with the simulation. Energy demand is defined in Tables 5.2 and 5.3, the input parameters regarding financial, and energy system's limitations are defined in Table 5.5, the definition of each parameter is well-described in chapter 4. Limitation on maximum generation capacities have already been reported for each region under

analysis in Table 5.4 and limitation on maximum injection will vary according to the transmission line connection the individual site is linked.

To test the tool and explore various scenarios, it will be outlined two different situations. The first scenario focuses on connecting to medium voltage transmission lines (220 kV), while the second scenario examines high voltage connection transmission lines (380 kV). By examining the limitations on injection, the results will demonstrate the disparity between low and high restrictions, and the subsequent impact on other analyzed metrics like self-sufficiency, self-consumption, and economic parameters.

Table 5.5: Input parameters for single-site simulation

Parameter	Units
MaxC_PV	MW
MaxC_WT	MW
Max_Injection	1480 MW
IRR	8%
Ele_price	24 c€/kWh
Sell_price	4 c€/kWh
uCostPV	650 €/kW
uCostWT	1000 €/kW
uCostStorage	300 €/kWh
Discharge_time	1 h
mCostPV	10 €/kW
mCostWT	0.0085 €/kWh
eNPV	1 €

The simulation will perform the optimization model for a single-site returning the optimum sizes for generation and storage capacities within an IRR higher or equal to 8% for each province over a 21-year period simulation. Financial parameters and costs were provided by the university of Cagliari, the values are shown in Table 5.5.

Visualization results are distributed from hourly to yearly resolution, in figure 5.6 it is shown an example of hourly profiles during a month of high production. By examining the figure, it is observed the fluctuations and patterns in production over the course of a day or weeks, providing valuable insights into the system's behavior. This feature potentially identifies peak production periods or any recurring patterns, as the one regarding the BESS

By implementing the optimization model with the various decision variables and

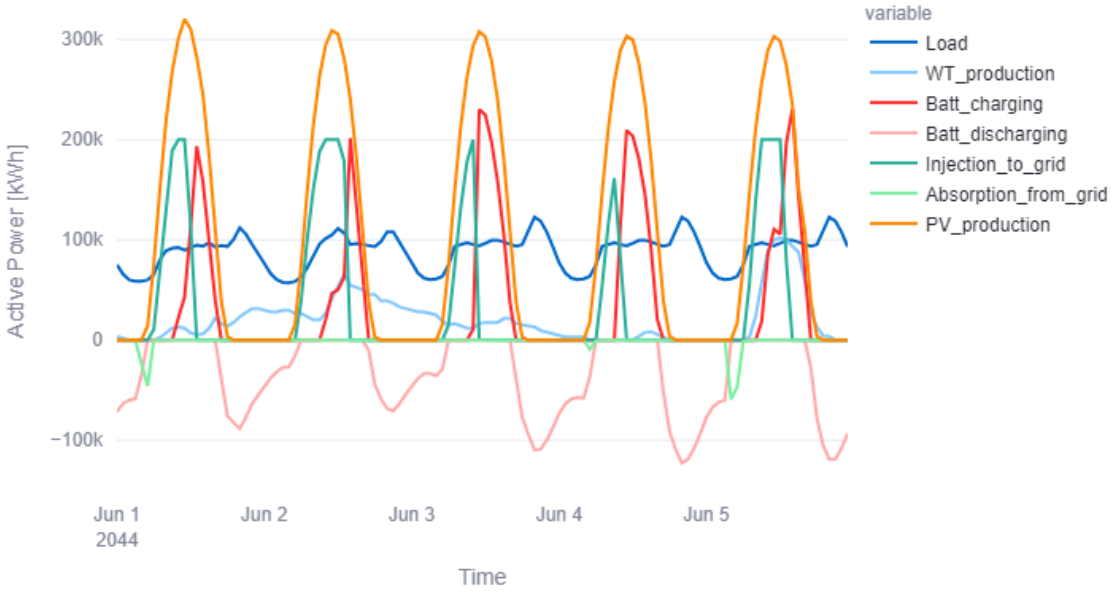

Figure 5.6: General hourly profiles during high production period.

constraints it was possible to reconstruct from the RES production and the energy demand the other parameters composing the energy system, for instance the power absorption or power battery. In fact, this is the powerful feature this software provides, the solver will reconstruct the optimal values for all the decision variables inside a feasible area where all the constraints are met. As a demonstration, in Figure 5.7 it is reported for a week period the battery management. S_capacity stands for the decision variable related to optimal storage capacity, and where the light blue profile is the energy inside the battery, as noticed it respects the conditions of limits on SOC_{min} and SOC_{max} and follows the profiles of generation for charging when high production or discharging power in cases of low production.

In terms of performance, the converge times the solver takes to find an optimal solution were satisfactory. Even though, the model has a big range of decision variables and constraints with an hourly resolution for a 21 year-period, the linearization of the model supported the fast convergence. For each site simulated within a period ranging from 1 to 2 minutes it was possible to obtain the optimal values for generation and storage capacities, and reconstruct all the variables that the renewable energy system comprises.

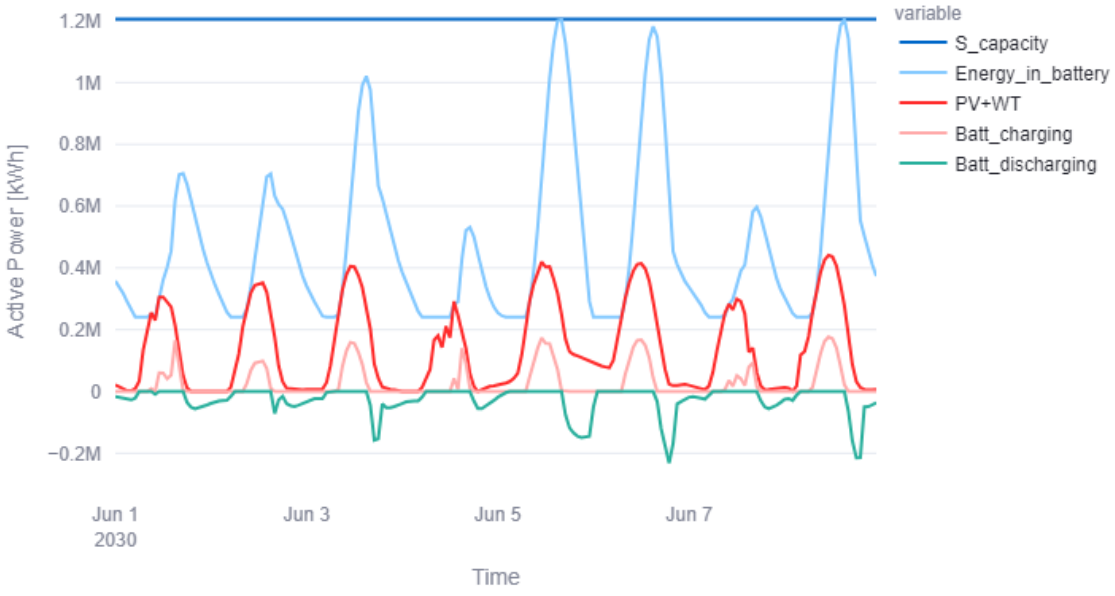

Figure 5.7: General battery management profiles

For simplicity, in the following cases only two regions will be depicted for their graphical representation, because the tool capability allows the data visualization site by site. However, at the conclusion of each energy scenario, it will be provided a results summary table to compare the regions under analysis. This table will highlight the levels of SS achieved in each scenario, providing valuable insights for decision-making regarding Sardinia's potential reliance on RES generation for decarbonizing the island in between 2030 and 2050 timeframe.

The energy landscape for Sardinia is promising due to all the facts described at the beginning of the chapter, specially in regards the plans for grid capacity expansion the island has embarked. Accordingly, for the periods under evaluation Sardinia has a bright potential on supporting energy transition, this is why makes it a suitable case study to test the tool. The energy scenarios that will be study were chosen based on the maximum power injection to the grid because it represents a direct factor for maximizing SS, the limitations in grid capacity is in fact, an energy transition bottleneck regarding RES penetration in emerging energy systems.

5.3.1 Limit on injection at medium voltage transmission lines

The two regions selected for the single site graphical results are composed by OT and CA, both with different levels of energy consumption inside Sardinia, with a proportion of 32% for Cagliari and 4% for Olbia. The results will show the contrast for the energy system behavior and reconstruction of the complementary variables, according to the connection at medium voltage (220 kV) transmission lines, with an assumed value of 200 MW for maximum injection to grid.

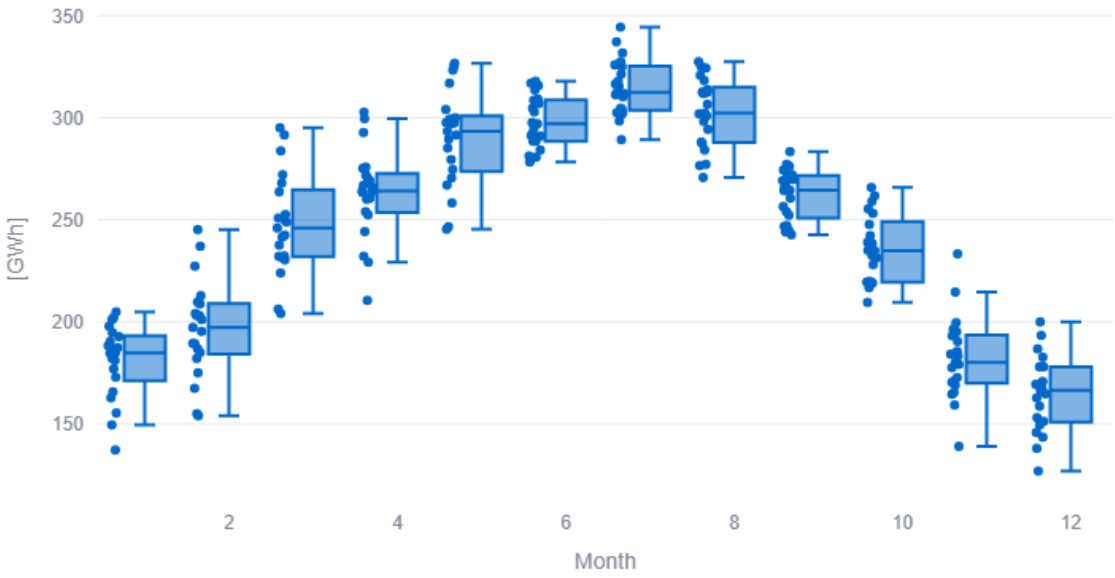

Figure 5.8: Cumulative monthly data distribution for PV production

To begin the analysis of energy production from photovoltaic (PV) and wind turbine (WT) sources, Figures 5.8 and 5.9 present the cumulative data distribution for both types of production over the evaluated time period. It is observed that the distribution for PV production exhibits a distinct pattern during the summer months, where there is a notable increase in PV energy production, indicating a higher generation of electricity from solar panels. In contrast, the distribution for WT production remains relatively constant throughout the years, due to the fact that relies on wind speed and availability, which can be more consistent throughout the year.

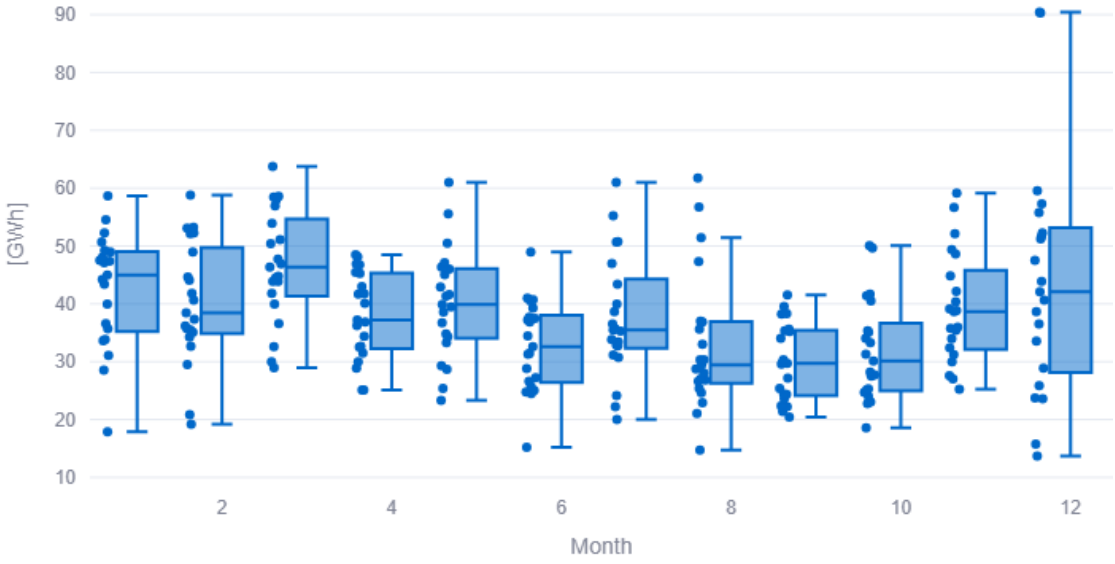

Figure 5.9: Cumulative monthly data distribution for WT production

The results are composed by plots from hourly to yearly resolution, due to the fact that the hourly G, u and T are given with real values variation for the 21 year-period, the tool provides accurate results. Which can be analyzed in its hourly original form or be re-sampled to analyze monthly, yearly profiles. Furthermore, enabling the program with the local database allowed going easily through all the energy scenarios simulated, due to the modularity approach the tool was developed on. Despite the huge size of each modelled region, the program handles to provide high quality resolution results.

Accordingly, the data visualization is capable of providing cumulative data plots as the ones represented in Figures 5.10 and 5.11 which represent the hourly cumulative profiles for the years 2030 and 2050 in the region of OT. This graphs help the user to analyzed the results and energy system's performance for the initial year and last year. As mentioned previously, the load is assume to increase constantly from the period in between 2030 and 2050. Additionally, the ageing factor for decrement on production from renewables is assumed 0.5% per year.

The hourly plots place in evidence the hours with higher production from renewables, which accordingly for *PV_production* the generation is maximum during

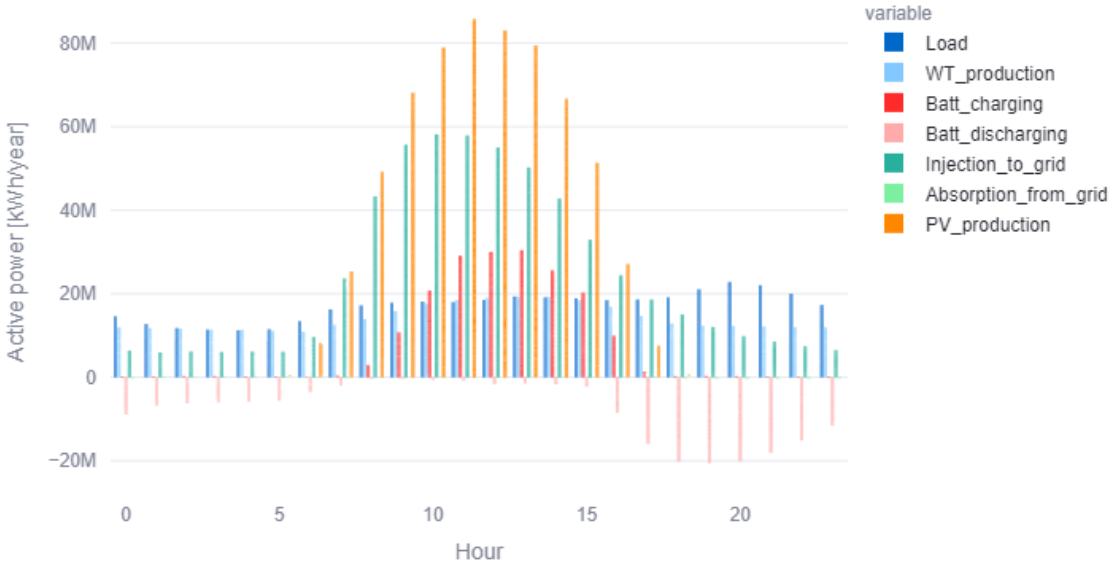

Figure 5.10: OT hourly cumulative energy profiles for year 2030

sun hours and for *WT_production* has a more constant behaviour throughout the day. During periods of over production, power injection to the grid and power charging for the battery takes place, and then power discharging during the night periods of low production. Moreover, no power absorption was required to supply the energy demand for the year 2030 in OT, meaning 100% self-sufficiency for the first year.

Nevertheless, the results for the year 2050 drastically change in contrast with the first year of simulation. The 2050 load has almost triple the initial one, with higher demand during nights. Production from renewables decreased because of the aging factor, therefore the reliance from the grid absorption increased during night time significantly. Despite the high increment of energy demand for the year 2050 and that no more generation capacity were considered to be added during time, in 2050 according to the results the system can still satisfy the load with high level of self-sufficiency, see Table 5.6, in this sense being still able to inject power to the grid in periods of overproduction.

Additionally, when the data is resampled at a monthly resolution, it allows us to examine the behavior of key variables during each month and gain insights into their

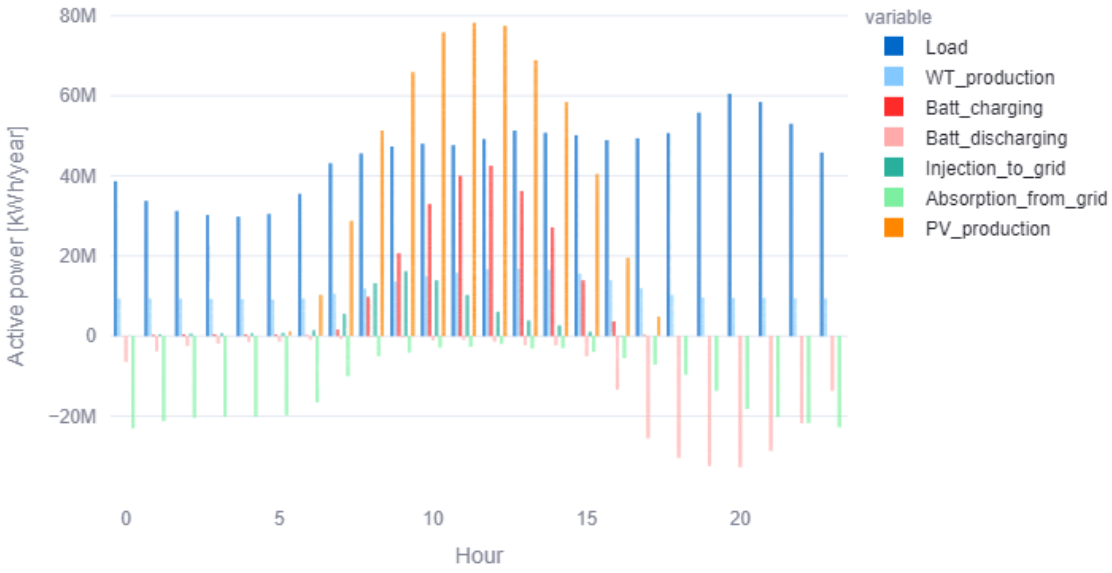

Figure 5.11: OT hourly cumulative energy profiles for year 2050

profiles. Figure 5.12 illustrates the profiles for the OT region, revealing a prominent emphasis on PV generation during the summer months. This dominance can be attributed to the higher generation capacity of PV compared to WT. Consequently, the power injected into the grid follows the pattern of PV generation, resulting in surplus electricity during the summer months. Conversely, the absorption of power from the grid is more pronounced during the winter months, indicating a greater reliance on grid power during that time. It is notable to mention, that the values of active power refer to the cummulative ones, meaning for the month 7 a total PV production of 1.5 GWh for the 21 year-period simulation.

By analyzing the monthly profiles of these variables, we can better understand the seasonal patterns and dynamics of energy generation and absorption in the OT region. This information can be valuable for decision-making and optimizing the utilization of renewable energy sources to meet the region's energy demands throughout the year.

The final graph to be analyzed presents the yearly profiles and provides a summary of power distribution between the energy system and the electric grid over a 21-year period as shown in Figure 5.13. The overall results indicate a substantial

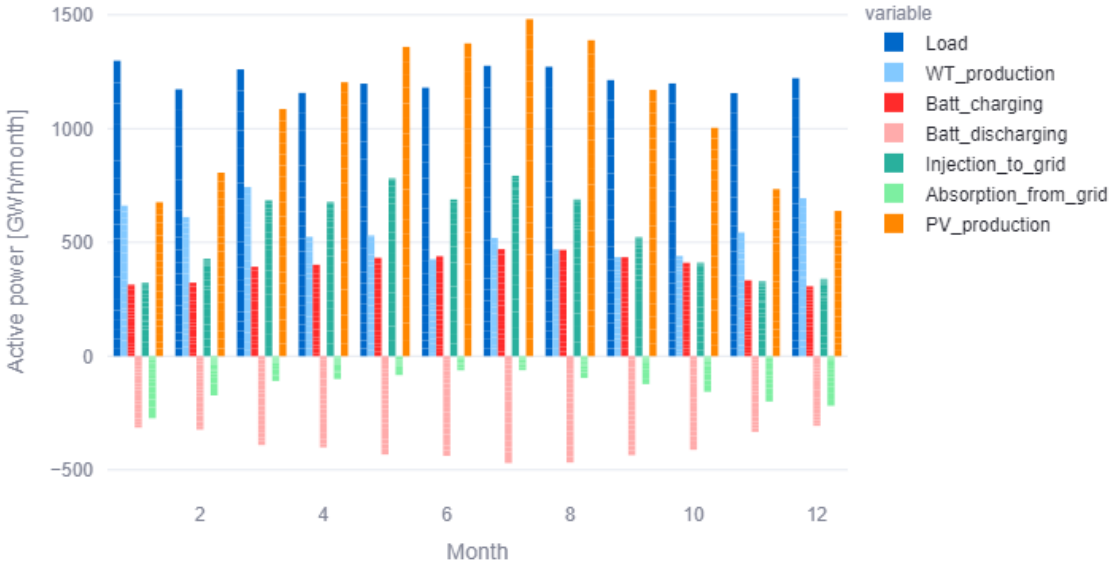

Figure 5.12: OT monthly cumulative profiles for 21 year period simulation

increase in energy demand throughout the simulation, starting from 400 GWh in the first year and reaching 1 TWh by 2050. At a certain point in the middle of the simulation, the energy load even surpasses the generation capacity of PV production.

However, the total renewable energy generation amounts to approximately 900 GWh, indicating a significant contribution from renewable sources. The power balance heavily favors local generation, as evident from the fact that power absorption from the grid is only notably required during the last five years of the simulation.

- $n\_PV = 433$ for a singular PV panel of 1 MW meaning an installation capacity for PV farm of 1.97 GW.
- $n\_WT = 62$ for a singular WT of 2 MW meaning a wind farm of 76 MW.
- $c_s = 1.2$MWh for storage capacity

These results demonstrate high levels of self-sufficiency SS at 89% and SC at 66% for Olbia, making it suitable for decarbonizing its energy system and relying

on renewable energy sources. Even when the maximum injection is limited to 200 MW for a medium voltage connection of 220 kV, the optimal capacities of the energy system still yield high levels of self-sufficiency and ensure a positive net present value (NPV), at the point that the overall power injection with respect to the load reaches 46%. These findings are reported in Table 5.6, and for the other 7 regions as well.

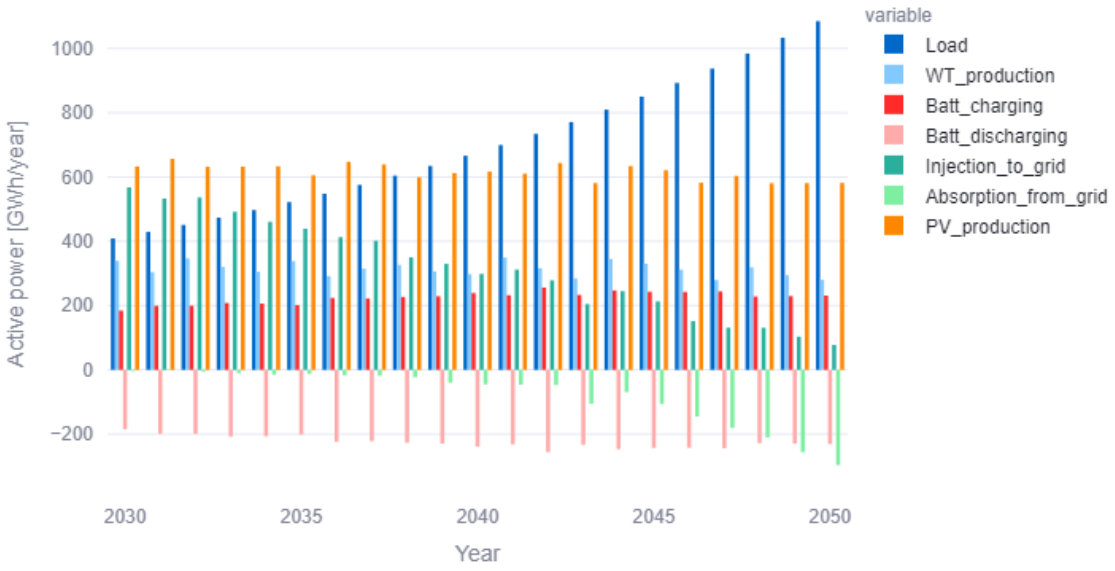

Figure 5.13: OT yearly cumulative profiles for 21 year period simulation

On the other hand, CA has higher energy demand which requires higher generation and storage capacities to fulfil the load, which starts from from 3 TWh in the first year and reaching 8 TWh by 2050. However, with the limitations on grid injection for medium voltage transmission lines, finding a optimal configuration for the energy system that satisfies the power balance and economic constraints it is more complicated than the previous case. Nevertheless, CA energy scenario reaches 63% of SS and 96% of SC, due to the fact that the overall power injection with respect the load only reaches 2% the RES generation is almost completely self consume, and the wasted power (curtailment) is only 2% as well.

While in the first year, the renewable energy plants primarily supply the load with minimal power absorption from the grid, by the year 2050, the system struggles to meet the energy needs and heavily relies on the grid for support. This indicates

a growing demand and potential challenges in maintaining self-sufficiency in the later years of the simulation if the limits on power injection remain the same.

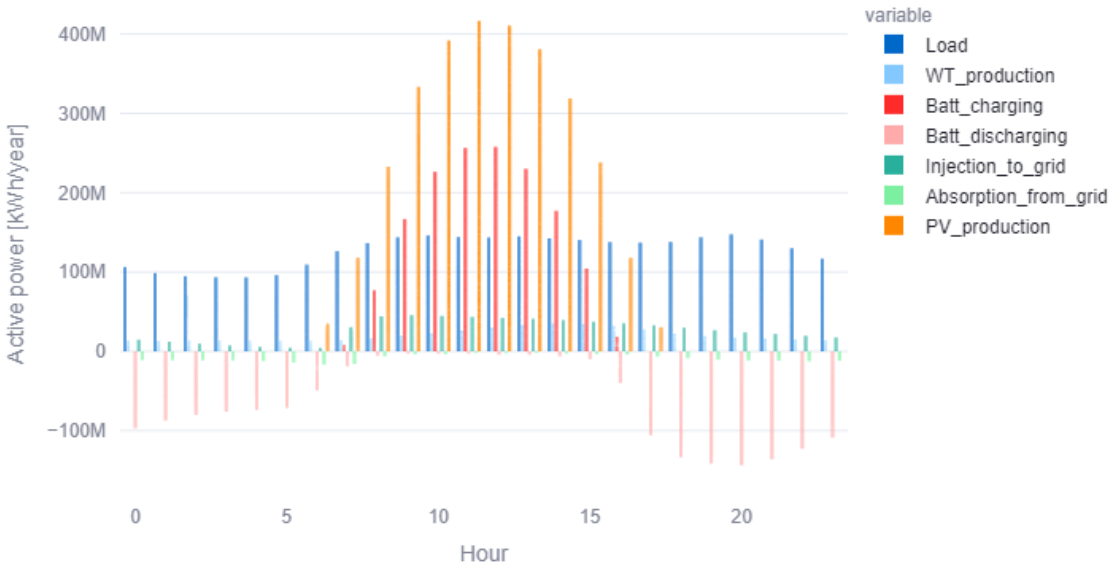

Figure 5.14: CA hourly cumulative energy profiles for year 2030

The optimal values that satisfied the CA energy model connected at medium voltage level are composed by:

- $n\_PV = 1965$ for a singular PV panel of 1 MW meaning an installation capacity for PV farm of **1.97 GW**.
- $n\_WT = 92$ for a singular WT of 2 MW meaning a wind farm of **184 MW**.
- $c_s = 7.16$ MWh for storage capacity.

Within the model and the electricity market, the primary means of recouping investments is through the sale of electricity to the grid. In the case of Cagliari, only 2% of the renewable energy generation was injected into the grid. As a result, the model prioritizes the installation of photovoltaic (PV) capacity, as it is typically more cost-effective compared to other energy components. In this sense the model

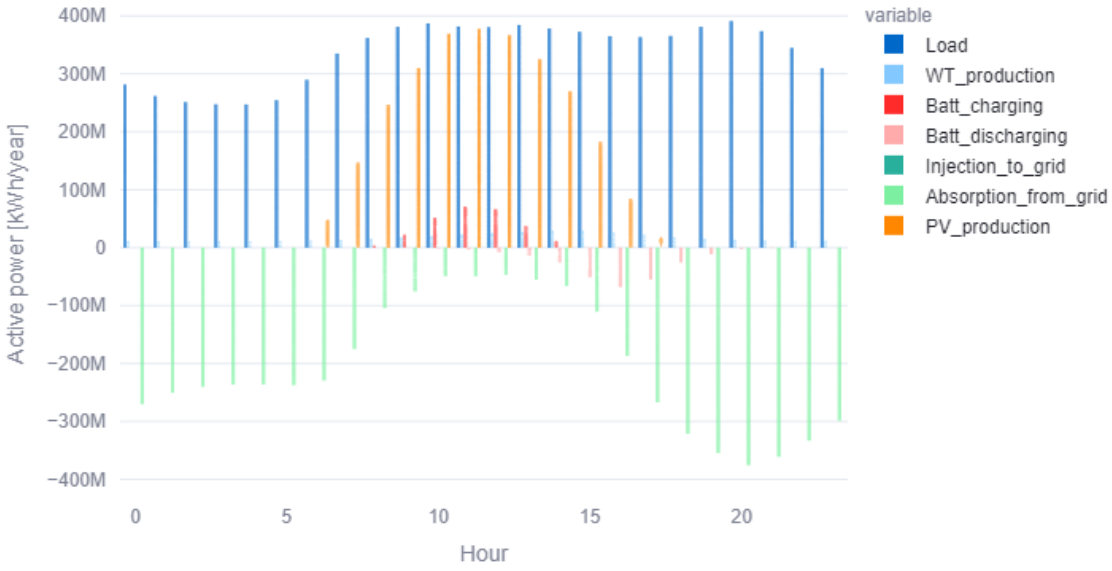

Figure 5.15: CA hourly cumulative energy profiles for year 2050

is capable of having a positive value for the NPV at the end of the simulation with a value of 630.000 €.

Monthly and yearly profiles in Figures 5.16 and 5.17 can better represent the challenges CA faces to supply its high energy demand during the simulation period. For instance, cumulatively, there is no month or year where PV production is higher than the energy consumption, and the reliance on power absorption from the grid starts to be highly significant after 8 years of plant's installation.

The monthly patterns further emphasize the dominant role of PV production in the overall renewable energy generation. This reliance on PV generation leads to a higher dependence on the grid during the winter season when solar irradiance is lower. As a result, the energy system must compensate for the reduced PV production by relying more heavily on grid power during these months.

These observations shed light on the challenges faced by CA in supplying its high energy demand while striving for renewable energy integration. The data suggests that additional measures, such as diversifying the renewable energy mix or upgrading the grid capacity that support the renewble penetration.

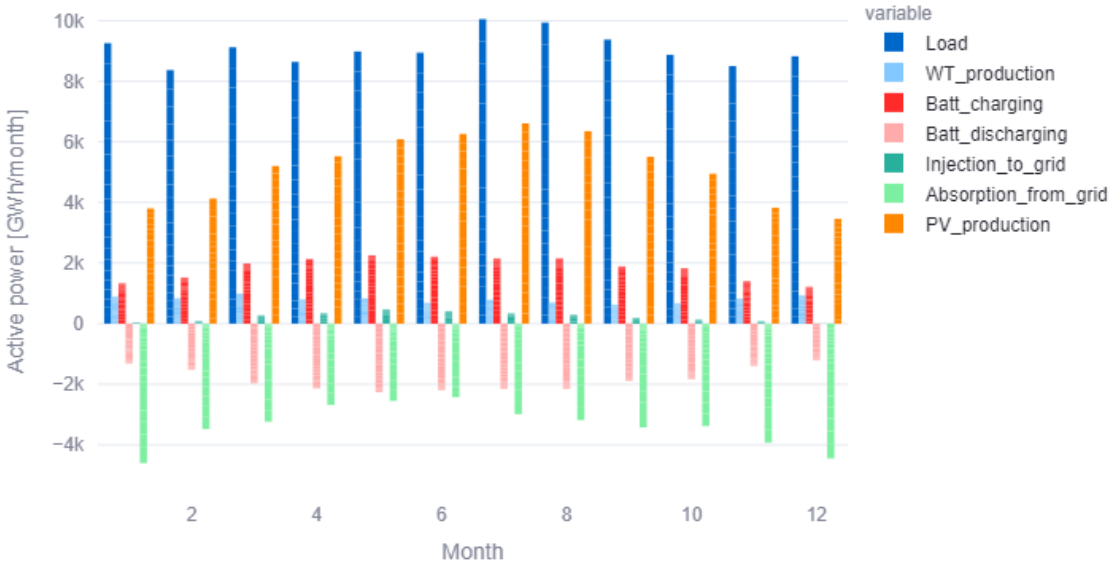

Figure 5.16: CA monthly cumulative profiles for 21 year period simulation

Nonetheless, it is worth mentioning that the simulation has been performed considering Sarlux out of the energy system, this is promising for the future energy landscape Cagliari has towards decarbonization. This could involve increasing the deployment of renewable energy technologies and the proper infrastructure to ensure their efficient penetration to the electrical grid.

In the following subsection, it will evaluated the case where the regions are connected to high voltage 380 kV transmission lines. This configuration enables a higher rate of power injection into the grid, allowing for increased integration of renewable energy sources. By changing connection to high voltage lines, sites can significantly enhance its renewable energy integration and overall system performance, specially in cases such as CA, SSS and CI with high energy demand to supply.

In Table 5.6, the simulation results for the key parameters of each province are presented, considering a connection to medium voltage with a maximum injection of 200 MW. The table provides an overview of the findings for each region.

One common trend observed across all regions is that PV generation predominates over WT production. This can be attributed to the cost-effectiveness of

installing PV panels compared to wind turbines. The regions prioritize PV installations due to their relatively lower costs and higher availability of solar resources. However, regions with higher energy demands exhibit lower levels of SS and require larger storage capacities, the higher storage capacity requirement also implies higher initial investment costs for these regions.

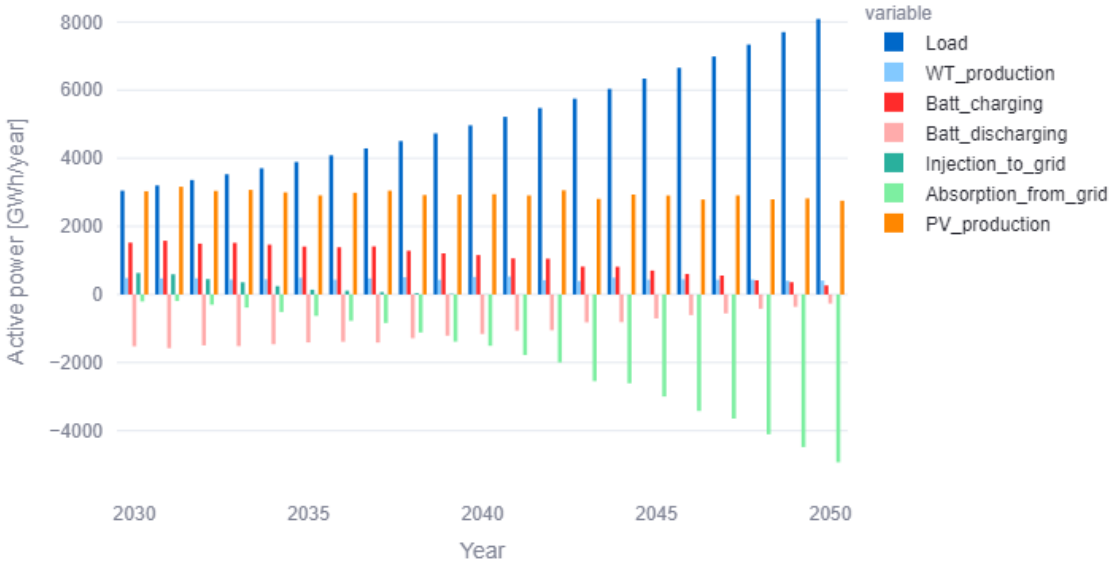

Figure 5.17: CA yearly cumulative profiles for 21 year period simulation

Undoubtedly, CA is the special case between the regions under analysis, it required the higher initial investment for the energy system installation, as its total installed generation capacity rounds the 2 GW and storage capacity 7.2 MWh. Due to its simulated energy system and low levels injection, CA out stands with the higher level of SC with respect to the others.

It will be explores how CA performs in a new case scenario with higher injection capabilities. By increasing the injection capacity, CA can potentially enhance its renewable energy integration and overall system performance. The following section examines the potential effects and benefits of this scenario.

Table 5.6: Simulation's summary table for Sardinia provinces with 200 MW as maximum power injection.

	OT	VS	NU	OG	CA	CI	OR	SS
Capacity results								
PV Capacity [MW]	433	531	719	362	1965	1266	853	1130
WT Capacity [MW]	124	76	70	74	184	130	144	178
Storage Capacity [MWh]	1.2	1.1	1.8	0.5	7.2	4.2	2.9	3.8
First year results								
RES production[GWh]	971	884	1153	652	3513	2115	1673	1915
Load [GWh]	408	403	664	183	3048	1868	1054	1696
Injection to grid [GWh]	567	486	494	471	630	438	627	356
Absorption from grid [GWh]	3	7	9	0	205	166	11	142
Last year results								
RES production[GWh]	861	804	1063	604	3161	1895	1503	1782
Load [GWh]	1085	1069	17620	487	8088	4957	2798	4501
Injection to grid [GWh]	143	89	18	222	0	0	0	0
Absorption from grid [GWh]	296	351	715	101	4925	3060	1292	2717
Metric results for 21 years								
Self-sufficiency	89%	85%	80%	81%	63%	62%	79%	63%
Self-consumption	66%	67%	80%	33%	96%	95%	87%	95%
Absorption/Load	11%	15%	20%	19%	37%	38%	21%	37%
Injection/Load	46%	41%	20%	111%	2%	3%	11%	3%
RES/Load	134%	126%	100%	201%	65%	65%	90%	66%
Economic results								
NPV after 21 years [M€]	10	4	5	7.41	0.63	1.7	11.9	13
Initial investment [M€]	654	648	913	403	2934	1806	1320	1700
IRR	8%	8%	8%	8%	8%	8%	8%	8%

5.3.2 Limit on injection at high voltage transmission lines

In this subsection the regions have been simulated connecting them to a high voltage transmission line, assuming 1000 MW of maximum power injection to the grid. The site representing the graphical analysis consists of CA, the region

inside Sardinia with higher energy needs. From figure 5.18 it can be noticed in advance the enormous difference with respect to the previous case, production from renewables during the first year of simulation overcomes load mainly by solar which has 2.4 GW of installed capacity. It is also evidenced the absence of reliance on the grid, locally generation predominated.

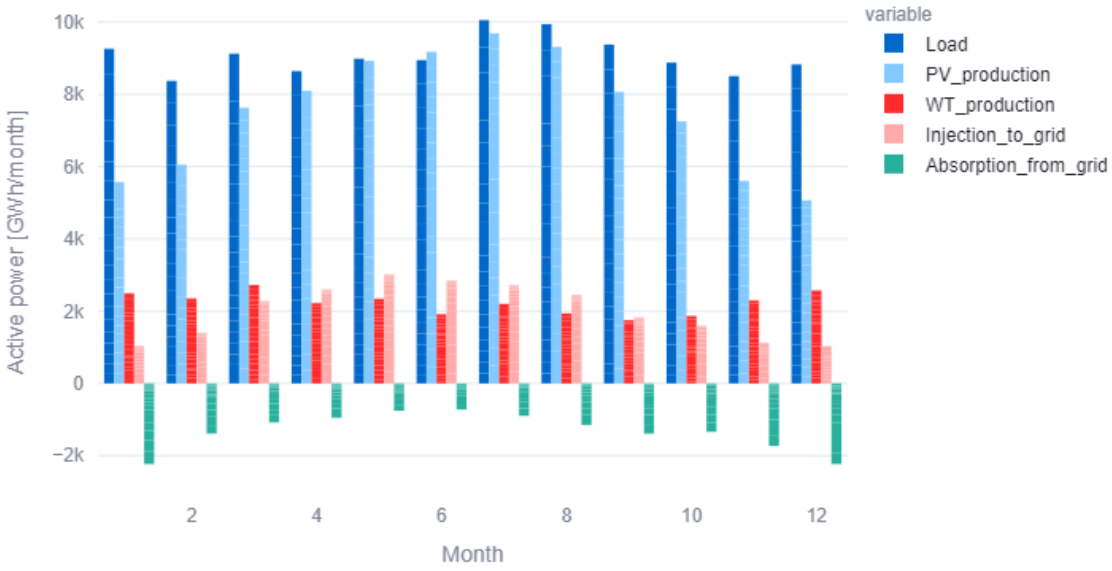

Figure 5.18: CA monthly cumulative profiles for 21 year period simulation, second case scenario

However, overproduction leads to increase waste energy, denominated as curtailment. For cases like this one of high penetration of renewable into the grid, the power that cannot be longer stored or injected results in energy wasted. CA for this case scenario obtained an 8% of curtailment, with only 15% of reliance from the grid and 22% of overall power injection.

At the end of the simulation, despite the high demand of Cagliari, the generation from renewables is capable of overcoming the energy need during the periods of sun hours. The profiles of power absorption show accordingly high demands during night times.

Cumulative monthly graphs also represent how the generation from renewables can withstand energy needs. The outcome shows a well-balanced energy scenario

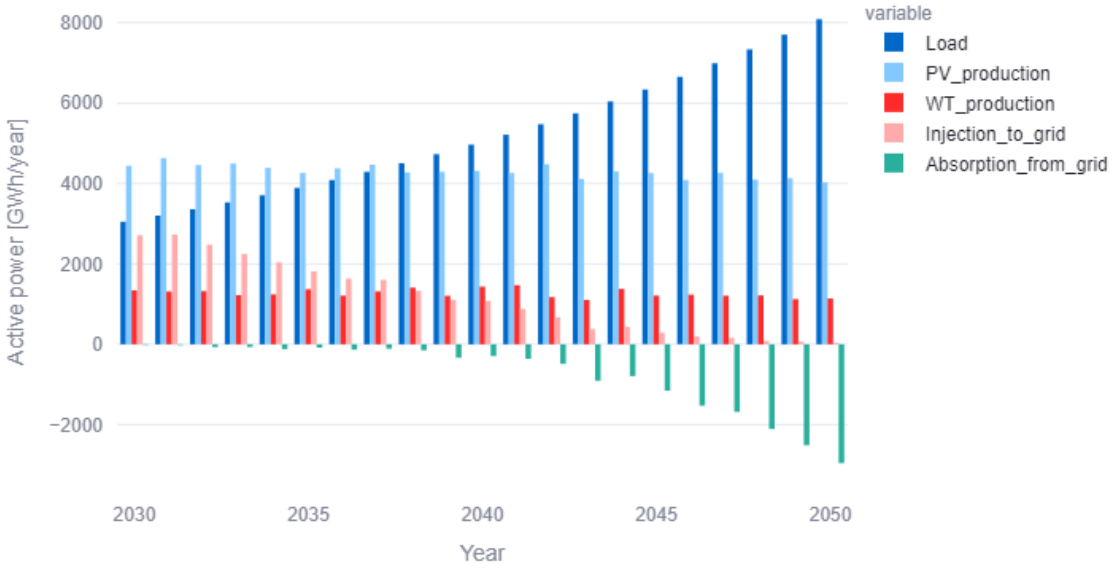

Figure 5.19: CA yearly cumulative profiles for 21 year period simulation

for Cagliari, as it has higher level of SS than the previous case (85%) and also keeping high levels of SC (79%). Generation from renewables encompasses a 108% rate.

5.4 Comments on results

The results for both simulations performed in the Sardinia case study, suggest that the regions with high levels of energy demand will achieve higher levels of SS and possible as the case of CA high levels of SC as well. Due to the fact higher levels of injection provides more positive cash flows, then more generation capacities can be installed, and still achieving positive values of NPV at the end of the simulation. On the other hand, regions with low demand connected to high voltage transmission lines will tend to oversize their generation capcities.

Table 5.7: Simulation's summary table for Sardinia provinces with 1000 MW as maximum power injection.

	OT	VS	NU	OG	CA	CI	OR	SS
Capacity results								
PV Capacity [MW]	863	1458	1458	848	2879	2131	1459	1904
WT Capacity [MW]	486	88	250	88	512	434	484	494
Storage Capacity [MWh]	1.17	1.14	1.8	0.49	9	5.3	3.2	4.7
First year results								
RES production[GWh]	2589	2097	2498	1414	5783	4027	3446	3554
Load [GWh]	408	403	664	183	3048	1868	1054	1696
Injection to grid [GWh]	2177	486	1834	1232	2713	2145	2383	1873
Absorption from grid [GWh]	0	7	0	0	15	0	0	0
Last year results								
RES production[GWh]	2256	804	2297	1306	5172	3541	3102	3311
Load [GWh]	1085	1069	17620	487	8088	4957	2798	4501
Injection to grid [GWh]	1293	1259	869	904	40	185	735	185
Absorption from grid [GWh]	117	230	332	84	2954	1598	430	1372
Metric results for 21 years								
Self-sufficiency	96%	92%	93%	93%	85%	87%	95%	87%
Self-consumption	27%	28%	43%	21%	79%	72%	51%	71%
Absorption/Load	4%	8%	7%	7%	15%	13%	5%	13%
Injection/Load	258%	235%	124%	343%	22%	34%	91%	36%
RES/Load	353%	327%	217%	436%	65%	121%	185%	122%
Economic results								
NPV after 21 years [M€]	9	4.2	5.9	6.72	1.03	2.65	9.6	11
Initial investment [M€]	1232	1214	1537	697	4287	2921	2077	2709
IRR	8%	8%	8%	8%	8%	8%	8%	8%

Chapter 6

Conclusion

In summary, the development of the tool, starting from the mathematical formulation of the optimization problem to its implementation, has achived satisfactory outcomes. The challenges related to computational costs were successfully addressed by fully linearizing the model and implementing it within Gurobi for solving the MILP problem. Despite the high-resolution input dataset and the numerous decision variables and constraints, the solver rapidly identified feasible regions and provided optimal configurations for the evaluated energy systems.

Integrating the Gurobi solver within the Python environment has facilitated the creation of different energy scenarios and their interactive visualization of results. It was made possible by the modular programming approach that was adopted and the automated local database, that fluently communicate within the front-end.

The powerful feature of the tool emphasizes on the hourly reconstruction of the decision variables the modelled energy system encompasses, by following the constraints the solver was capable of returning the optimal values that effectively minimizes reliance on the grid, thus maximizing SS. Accordingly, In the case study conducted for Sardinia, the model demonstrated its capability to adapt to different energy scenarios, as changes in the maximum power injection to the grid directly impacted the levels of self-sufficiency for a single-site. The outcome of the results suggested the connection to high voltage transmission lines to the regions with high demand levels. This highlights the model's versatility and its potential for informing decision-making processes in the energy sector.

Despite rigorous efforts and comprehensive analysis, the objective of implementing a multiple-site energy scenario for Sardinia could not be fully achieved.

The approach to interconnect regions through the electrical grid and also model the HVDC lines connecting the island to mainland, was expected to give more accurate results for an island or country level simulations. Nevertheless, the path has been delved providing the models to integrate the linear PTDF and the various constraints inside the single-site model.

Overall, the tool development has been successfully implemented for a single-site, achieving the objective to provide a software capable of easily construct energy scenarios to support decision-making and energy transition.

Appendix A

Appendix

A.1 Implementation code

```
class RegionData():
    'pvgis class to get hourly weatherdata and an attribute to pass from json to dataframe type'

    url = "https://re.jrc.ec.europa.eu/api/v5_2/seriescalc?"

    def __init__(self, province, region, lat, long, years):
        try:
            self.province = province
            self.region = region #input('Insert region name: ')
            self.latitude = lat #input('Insert latitude: ')
            self.longitude= long #input('Insert Longitude: ')
            self.start_year = '2005'
            self.end_year = '2020'
            print(self.end_year)

            self.final_url = self.url+ "lat=" + self.latitude + "&lon=" + self.longitude + "&startyear=" + self.start_year \
                    + "&endyear=" + self.end_year + "&optimalangles=1&outputformat=json&browser=1"


            regions.append(self.region)
        except:
            print("Error connecting to PVGIS API")
```

```
def set_load(df, increment, years):
    increment = increment
    #years = years

    energy_load_data = [df.Load]
    for year in range(1, years):
        energy_load = df.Load * (1 + increment) ** year
        energy_load_data.append(energy_load)

    total_energy_load = pd.concat(energy_load_data, ignore_index=True
    )

    return total_energy_load

def RES_generation(df, n_pv, n_wt):

    df['G(i)'] = df['G(i)']/1000 #irradiance in kW
    df = df.round(3)

    # PV production model
    df['PV_cell_temp'] = (df['T2m'] + (((c_eb.PV_NOCT-20)/0.8)*(df['G
    (i)'])))
    df['PV_eta_thermal'] = (1 + c_eb.PV_gamma_th * (df['PV_cell_temp'
    ]-c_eb.PV_T_stc))
    df.loc[df['G(i)'] < c_eb.PV_G_0, 'PV_DC'] = 0
    df.loc[df['G(i)'] < c_eb.PV_G_0, 'PV_production'] = 0
    df.loc[df['G(i)'] > c_eb.PV_G_0, 'PV_DC'] = (c_eb.
    PV_nominal_power * n_pv * ((df['G(i)'] - c_eb.PV_G_0)/c_eb.
    PV_G_STC) * (df['PV_eta_thermal'] * c_eb.PV_eta_mix))
    df.loc[df['G(i)'] > c_eb.PV_G_0, 'PV_production'] = (-(1+c_eb.
    PV_K_lin) + ((1 + c_eb.PV_K_lin)**2 + (4 * c_eb.PV_K_quad) * ((df
    ['PV_DC']) - c_eb.PV_Po))**0.5) / (2 * c_eb.PV_K_quad)

    # WT production model
    df['U_w'] = df['WS10m'] * (c_eb.WT_numerator / c_eb.
    WT_denominator)
    df['U_w'].loc[df.U_w > max(c_eb.lst_wind_speed)] = max(c_eb.
    lst_wind_speed) # limit if U_w exceeds wind speed WT power curve
    WT_power_interpol = scipy.interpolate.interp1d(c_eb.
    lst_wind_speed, c_eb.lst_pow_Gamesa)
    df['WT_production'] = WT_power_interpol(df['U_w']) * n_wt
    df.drop(['PV_DC','G(i)','T2m','WS10m','U_w','PV_cell_temp','
    PV_eta_thermal'],axis=1,inplace=True)

    n=8760
    n_years = int(len(df)/n)
    cont_year = 1

```

```
    df['Time'] = pd.to_datetime(df['Time'], format='%Y-%m-%d %H:%M:%S',  errors = 'coerce')
    rows_with_errors = df[df['Time'].isnull()]

    start_year = df['Time'].dt.year.min() + 1

    end_year = start_year + n_years
    ageing = float(0.005)
    for year in range(int(start_year), int(end_year)):
        df.loc[df['Time'].dt.year == year, 'PV_production'] *= (1 - ageing * cont_year)
        df.loc[df['Time'].dt.year == year, 'WT_production'] *= (1 - ageing * cont_year)
        cont_year += 1

    return df
```

```
class DAO():
    'Class Data Access Operator'

    def __init__(self):
            try:
                self.engine = create_engine("mysql+pymysql://{user}:{pw}@localhost/{db}"
                                            .format(user="root",
                                                    pw="",
                                                    db="electrifysardinia"))

                self.conn = self.engine.connect()


            except Error as ex:
                print("Error : {0}".format(ex))
```

```
@st.cache_data
def site_selection():

    dao = DAO()
    table = 'new_case'
    df_select = dao.select_distinct(table)
    print(df_select)
    default_values = {

        "Max_#_PV": 1e7,
        "Max_#_WT": 1e7,
```

```
        "Max_Injection": 2e5,
        "Discount_rate": 0.08,
        "Ele_price": 0.24,
        "Sell_price": 0.04,
        "uCostPV": 650,
        "uCostWT": 1000,
        "uCostStorage": 300,
        "Discharge_rate": 1,
        "mCostPV": 10,
        "mCostWT": 0.0085,
        "eNPV": 1

    }

    df_inputs = pd.DataFrame(index=range(len(df_select)), columns=
    default_values.keys(), dtype=float)
    df_inputs.fillna(default_values, inplace=True)

    editable_df = pd.concat([df_select, df_inputs], axis=1)


    return editable_df
```

```
import streamlit as st
import plotly.express as pt
from DB.connector import DAO
import datetime

@st.cache_data
def setdata():
    dao = DAO()
    table = "high_voltage"
    df_H = dao.request(table)

    df_H = df_H.dropna()

    df_M = df_H.groupby(["Region"]).resample('M').sum(numeric_only =
    True)#resampling df for monthly plots
    df_Y = df_H.groupby(["Region"]).resample('Y').sum(numeric_only =
    True)

    df_Y['NPV_cum2'] = df_Y['NPV'].cumsum()
    numeric_df = df_Y.select_dtypes(['float', 'int']) #select numeric
     cols for both df
    numeric_df_orig = df_H.select_dtypes(['float', 'int'])
    numeric_cols = numeric_df.columns
    numeric_cols_orig = numeric_df_orig.columns
```

```
22
23      region_column = df_H['Region'] #unique value of regions in order
        to use region dropdown list
24      unique_region = region_column.unique()
25
26      return df_H,numeric_cols_orig, unique_region, numeric_cols, df_M
        ,df_Y
27
28  df,numeric_cols_orig, unique_region, numeric_cols, df_M, df_Y  =
        setdata()
```

```
1   import gurobipy as gp
2   from gurobipy import GRB
3
4   def optimal_values(df,opt_data):
5
6       years = 25
7       le = (8760 * years) - 1  #to control the optimization time,
        higher than the input length will be ignored
8       le = min(le, len(df))
9       df = df.loc[0:le]
10
11      PV_prod = df['PV_production']
12      WT_prod = df['WT_production']
13      Load = df['Load']
14
15      # Create the model #
16      m = gp.Model("Max_SS_Min_Absorption")
17
18      # Define the variables #
19
20      # Undependent of time
21      n_pv = m.addVar(lb = mpv, ub = opt_data['Max_#_PV'], vtype = gp.
        GRB.CONTINUOUS, name="number_of_pv")
22      n_wt = m.addVar( lb = mwt , ub = opt_data['Max_#_WT'], vtype=gp.
        GRB.CONTINUOUS, name="number_of_wt")
23      c_s = m.addVar( lb = mcs , vtype=gp.GRB.CONTINUOUS, name="
        Storage_capacity")
24
25      # Power generation
26      PG = n_pv*PV_prod + n_wt*WT_prod
27
28      # Dependent of time
29      # Power sharing Variables
30      EB_t= [m.addVar( vtype = gp.GRB.CONTINUOUS, name="
        Energy_in_battery")for i in range(len(Load))]
```

```
31      Pb_t = [m.addVar(lb = -GRB.INFINITY, vtype = gp.GRB.CONTINUOUS,
        name="Power_battery")for i in range(len(Load))]# Charging or
        discharging power
32      inj_t = [m.addVar( lb = 0, ub = opt_data.Max_Injection , vtype =
        gp.GRB.CONTINUOUS, name="Injection_to_grid")for i in range(len(
        Load))]
33      abs_t = [m.addVar( lb = -GRB.INFINITY, ub = 0 , vtype = gp.GRB.
        CONTINUOUS, name="Absorption_from_grid")for i in range(len(Load))]
34      Pc_t = [m.addVar( lb = 0, vtype = gp.GRB.CONTINUOUS, name="
        Curtailment")for i in range(len(Load))]
35
36      return
```

Bibliography

[1] Vaclav Smil. *Energy and Civilization: A History*. Cambridge, MA: MIT Press, 2017. ISBN: 978-0-262-03546-5 (cit. on p. 1).

[2] Wang Qiao. «Understanding the impact on energy transition of consumer behavior and enterprise decisions through evolutionary game analysis». In: *Sustainable Production and Consumption* (2021) (cit. on p. 1).

[3] Alessandro Ciocia. «Optimal Power Sharing between Photovoltaic Generators, Wind Turbines, Storage and Grid to Feed Tertiary Sector Users». In: (2017) (cit. on pp. 2, 20, 25–29, 39).

[4] URL: `https://corporate.enel.it/en/stories/a/2022/02/electrification-sardinia-multi-stakeholders-un-energy-compact` (cit. on pp. 2, 58).

[5] European commission. *Financing the green transition: The European Green Deal Investment Plan and Just Transition Mechanism*. URL: `https://ec.europa.eu/commission/presscorner/detail/en/ip_20_17` (cit. on p. 3).

[6] Iea. *Global Electricity Generation by technology, 2015, 2021 and 2027 –nbsp;charts – Data amp; Statistics*. URL: `https://www.iea.org/data-and-statistics/charts/global-electricity-generation-by-technology-2015-2021-and-2027` (cit. on pp. 4, 5).

[7] Asad Ullah. «A threshold approach to sustainable development: Nonlinear relationship between renewable energy consumption, natural resource rent, and ecological footprint.» In: *Journal of environmental management* (2021) (cit. on p. 3).

[8] A. A. Chen. «Pathways to climate change mitigation and stable energy by 100% renewable for a small island: Jamaica as an example». In: *Renewable Sustainable Energy Reviews* (2020) (cit. on p. 3).

[9] A. Tleppayev. «Relation of technology and urbanization with electricity consumption in Kazakhstan». In: *Economic Annals-I* (2020) (cit. on p. 4).

[10] Md Shahriar Mahbub. «Development of innovative tools for multi-objective optimization of energy systems». In: (Jan. 2017) (cit. on p. 4).

[11] European commission. *Best practices on Renewable Energy Self-consumption*. 2015. URL: https://eur-lex.europa.eu/legal-content/EN/TXT/PDF/?uri=CELEX:52015SC0141 (cit. on p. 6).

[12] M.B.; Prodanovic Téllez Molina. *M. Profitability assessment for self-sufficiency improvement in grid-connected non-residential buildings with on-site PV installations.* 2013 (cit. on p. 6).

[13] (Accessed on 24/03/2023. URL: http://www.senato.it/application/xmanager/projects/leg18/attachments/%20documento_evento_procedura_commissione/files/000/000/945/2018_12_21_-_RSE.pdf (cit. on p. 6).

[14] Alessandro Ciocia, Angela Amato, Paolo Di Leo, Stefania Fichera, Gabriele Malgaroli, Filippo Spertino, and Slavka Tzanova. «Self-consumption and self-sufficiency in photovoltaic systems: Effect of grid limitation and storage installation». In: *Energies* 14.6 (2021), p. 1591. DOI: 10.3390/en14061591 (cit. on pp. 6–8, 10, 31).

[15] Esther Mengelkamp. «A blockchain-based smart grid: towards sustainable local energy markets». In: *Computer Science - Research and Development* (2018) (cit. on p. 6).

[16] S. Salkuti. «Comparative analysis of electrochemical energy storage technologies for smart grid». In: *TELKOMNIKA Telecommunication Computing Electronics and Control* (2020) (cit. on p. 7).

[17] SBC Energy Institute. *Hydrogen-Based Energy Conversion - More than Storage: System Flexibility.* 2014 (cit. on pp. 7, 8).

[18] Rossi M. Viganò G.Moneta D. Clerici D. Carlini C. *Analysis of active power curtailment strategies for renewable distributed generation.* 2016 (cit. on p. 9).

[19] *A microgrid energy management system with demand response for providing Grid Peak Shaving.* 2016 (cit. on p. 9).

[20] Tobias Gybel Hovgaard. «MPC for wind power gradients — utilizing forecasts, rotor inertia, and central energy storage». In: *2013 European Control Conference (ECC)* (2013) (cit. on p. 9).

[21] Yanbin Li. «An Analysis of the Multi-Criteria Decision-Making Problem for Distributed Energy Systems». In: *Energies* (2018) (cit. on p. 11).

[22] F. Cavallaro. «Multi-criteria decision aid to assess concentrated solar thermal technologies». In: *Renewable Energy* (2009) (cit. on p. 11).

[23] National Instruments. *Wind turbine control methods.* (Accessed on 24/03/2023. URL: https://www.ni.com/en/solutions/energy/condition-monitoring/wind-turbine-control-methods.html (cit. on pp. 18, 19, 21, 28).

[24] Jean-Marie Tarascon Bruce Dunn Haresh Kamath. *Electrical Energy Storage for the Grid: A Battery of Choices*. 2011 (cit. on pp. 22–24).

[25] Vito Bongermino. «Pianificazione della generazione da fotovoltaico ed eolico con accumulo elettrochimico: i casi studio della Turchia, Uzbekistan e Kazakhstan». In: (Oct. 2020) (cit. on p. 25).

[26] IEA. *Innovation Gaps IEA Paris*. 2019. URL: https://www.iea.org/reports/innovation-gaps (cit. on p. 27).

[27] P Di Leo F Spertino F Corona. «Limits of advisability for masterslave configuration of DC/AC converters in photovoltaic systems». In: *IEEE Journal of Photovoltaics vol 2* (2012) (cit. on p. 27).

[28] URL: https://joint-research-centre.ec.europa.eu/pvgis-online-tool/getting-started-pvgis/api-non-interactive-service_en (cit. on pp. 27, 28, 41).

[29] Corona F Spertino F Ciocia A. «Experimental procedure to check the performance degradation on site in grid connected photovoltaic systems». In: *IEEE Photovoltaic Specialists Conference Denver Colorado* (2014) (cit. on p. 27).

[30] C Kral M Einhorn V Conte and J Fleig. «Comparison of electrical battery models using a numerically optimized parameterization method». In: *IEEE Vehicle Power and Propulsion Conference Chicago* (2011) (cit. on p. 29).

[31] I Batarseh A H Hussein. «An overview of generic battery models». In: *IEEE Power and Energy Society General Meeting, San Diego USA* (2011) (cit. on p. 29).

[32] Alexandre Oudalov. «Energy Storage in Electric Power Systems - Integration of Renewable Energy Sources». In: *ABB Switzerland, Corporate Research* (2015) (cit. on p. 30).

[33] E Lorenzo J Muñoz F Martinez Moreno. «On-site characterization and energy efficiency of grid-connected PV inverters». In: *Progress in Photovoltaics: Research and Applications* (2011) (cit. on p. 30).

[34] D G Luenberger and Y Ye. «Linear and Nonlinear Programming». In: *Third Springer* (2008) (cit. on pp. 32, 36).

[35] *pandas 2.0.2 documentation*. URL: https://pandas.pydata.org/docs/ (cit. on p. 44).

[36] URL: https://docs.sqlalchemy.org/en/20/ (cit. on p. 44).

[37] URL: https://numpy.org/doc/ (cit. on p. 44).

[38] URL: https://docs.scipy.org/doc/scipy/ (cit. on p. 44).

[39] Aug. 2022. URL: https://www.gurobi.com/documentation/ (cit. on pp. 45, 48).

[40] URL: https://docs.streamlit.io/ (cit. on p. 45).

[41] URL: https://plotly.com/python/ (cit. on p. 45).

[42] URL: https://www.enel.com/company/stories/articles/2021/07/electrification-green-sardinia-italy-2030 (cit. on p. 58).

[43] Chiara Volonté. *Terna: Tutto Pronto per tyrrhenian link, La più grande opera industriale in Italia da decenni*. Jan. 2023. URL: https://www.industriaitaliana.it/terna-tyrrhenian-link-elettrodotto-hvdc-energia/ (cit. on pp. 59, 61).

[44] TERNA. «Rapporto adeguatezza italia». In: (2021). URL: https://download.terna.it/terna/Terna_Rapporto_Adeguatezza_Italia_2021_8d9a51d27ad741c.pdf (cit. on pp. 59, 60, 63).

[45] EMaps. *Impatto climatico per area*. visited on 2023. URL: https://app.electricitymap.org/zone/IT-SAR?wind=true%5C&solar=false (cit. on p. 60).

[46] TERNA. *Rapporto statistico regionale 2020*. visited on 2023. URL: https://download.terna.it/terna/Statistiche%5C%20Regionali_2020_8da3e688a4231ad.pdf (cit. on p. 61).

[47] entsoe. «Grid map». In: (visited on 2023). URL: https://www.entsoe.eu/data/map/ (cit. on p. 62).

[48] Marina Verrascina. «Energy transition of the Sardinia region through energy system modelling with the Calliope framework». In: (2022) (cit. on p. 65).